

A SON-Based Algorithm for the Optimization of Inter-RAT Handover Parameters

Ahmad Awada, *Member, IEEE*, Bernhard Wegmann, Ingo Viering, *Member, IEEE*, and Anja Klein, *Member, IEEE*

Abstract—First, the deployment of the Long-Term Evolution (LTE) system will be concentrated on areas with high user traffic overlaying with the legacy second-generation (2G) or third-generation (3G) mobile system. Consequently, the limited LTE coverage will result in many inter-radio access technology (RAT) handovers from LTE to 3G systems and *vice versa*. Trouble-free operation of inter-RAT handovers requires the optimization of the handover parameters of each cell in both RATs. The current network planning and optimization methods provide a fixed network-wide setting for all the handover parameters of the cells. Cells that later show considerable mobility problems in operation mode are manually optimized with the aid of drive tests and expert knowledge. This manual optimization of the handover parameters requires permanent human intervention and increases the operational expenditure (OPEX) of the mobile operators. Moreover, the interoperability of several RATs increases further the parameter space of the handover parameters, which makes the manual optimization difficult and almost impracticable. To reduce OPEX and to achieve a better network performance, we propose in this paper a self-optimizing algorithm where each cell in a RAT updates its handover parameters in an autonomous and automated manner depending on its traffic and mobility conditions. The proposed algorithm uses a feedback controller to update the handover parameters as a means to providing a steady improvement in the network performance. In the context of control theory, the feedback controller consists of a proportional control block, which regulates the change in the magnitude of each handover parameter, and a gain scheduler, which modifies the parameters of the proportional control block depending on the mobility conditions in each cell. To benchmark the design of the proposed algorithm, we apply two general and nonself-optimization algorithms: Taguchi's method and simulated annealing to optimize the handover parameters. Simulation results show that the proposed self-optimizing algorithm reaches a stable optimized operation point with cell-specific handover parameter settings, which considerably reduce the number of mobility failure events in the network, compared with three fixed settings for the handover parameters. Moreover, it is presented that the proposed self-optimizing algorithm outperforms Taguchi's method and simulated annealing when applied to a mobility robustness optimization (MRO) problem.

Index Terms—Inter-radio access technology (RAT) optimization algorithm, mobility robustness optimization (MRO), self-organizing network (SON).

I. INTRODUCTION

THE CONTINUING increase in the demand for high-speed communication services requires mobile operators to deploy new radio access technologies (RATs) overlaying with legacy technologies [1]. The coexistence of multiple RATs offers mobile operators a powerful means to match network resources to different application requirements and to meet users' demands [2]. To exploit this variety of RATs and to provide users with the best quality of service, the handover parameters of base stations (BSs) belonging to different RATs have to be mutually optimized.

A typical approach to configuring the inter-RAT handover parameters is to determine the best default network-wide parameter setting during the network planning phase where each cell in a RAT applies the same handover parameters. This approach is simple; however, it does not yield the best network performance because the real irregular network layout requires a cell-specific adaptation of the handover parameters [3]. Therefore, in a following optimization phase during the network operation, mobile operators try to optimize the handover parameters of those cells where mobility problems are detected. This manual optimization is expensive as it needs permanent human intervention and the performance of drive tests, which increase operational expenditure (OPEX) [4]. For this reason, self-organizing networks (SONs) are foreseen in upcoming standards [5] to optimize the inter-RAT handover parameters in an automated manner.

The research topics of intra-RAT mobility robustness optimization (MRO) in a Long Term Evolution (LTE) system [6]–[10] and inter-RAT MRO between second-generation (2G) and third-generation (3G) systems [3], [4] have been extensively discussed in the literature. However, few papers deal with the inter-RAT MRO between the LTE and 3G or 2G mobile communication systems. The introductory study in [11] highlights the difference between intra-LTE and inter-RAT handovers and analyzes the impact of LTE and 3G handover parameters on network performance using simulative investigation. The work in [12] focuses on defining a general protocol run by the newly deployed RAT, e.g., LTE, which renders a simple cell-pair (i.e., (LTE, 3G) cells) optimization of any inter-RAT configuration parameters scalable in the whole LTE network. The defined protocol works for any type of inter-RAT configuration parameters and is not specifically designed for the inter-RAT handover parameters of LTE and 3G

Manuscript received May 29, 2012; revised September 5, 2012 and December 13, 2012; accepted February 10, 2013. Date of publication March 8, 2013; date of current version June 12, 2013. The review of this paper was coordinated by Prof. Dr. F. Gunnarsson.

A. Awada is with the Department of Communication Technology, Darmstadt University of Technology, Darmstadt 64289, Germany (e-mail: ahmad.awada.ext@nsm.com).

B. Wegmann is with Nokia Siemens Networks, Radio Systems, 81541 Munich, Germany.

I. Viering is with Nomor Research GmbH, 81541 Munich, Germany and also with the Technical University of Munich, 80333 Munich, Germany.

A. Klein is with the Communications Engineering Laboratory, Darmstadt University of Technology, 64289 Darmstadt, Germany.

Color versions of one or more of the figures in this paper are available online at <http://ieeexplore.ieee.org>.

Digital Object Identifier 10.1109/TVT.2013.2251923

systems. Moreover, the latter work does not specify or describe the algorithm needed for optimizing the inter-RAT handover parameters of LTE and 3G systems in a cell-pair manner.

In this paper, we propose a new SON-based algorithm for the optimization of inter-RAT handover parameters of LTE and 3G systems. The algorithm is run by each cell in both RATs in an autonomous and automated way. Each cell updates its handover parameters based on the values of predefined key performance indicators (KPIs), which capture the number and the type of mobility failure events in each cell. The changes in the magnitude of the handover parameters of each cell are determined by a feedback controller [13]. In the vocabulary of control theory, the two main components of the feedback controller are the proportional control block [13] and the gain scheduler [14], [15]. The change in the magnitude of each handover parameter is determined by the first control block and is proportional to a predefined error signal. The gain scheduler alters the behavior of the proportional control block by modifying its parameters [14], [15] depending on the mobility conditions in each cell. In addition to the new proposed self-optimizing algorithm, we apply two other well-known optimization methods: Taguchi's method [16] and simulated annealing [17] to optimize the inter-RAT handovers parameters of LTE and 3G systems. Simulated annealing is an optimization method that has been extensively used in many engineering problems [18], [19]. Taguchi's method is another promising optimization method that was first developed for the optimization of manufacturing processes [20] and has been recently introduced to wireless mobile communication field in [21]–[25]. Taguchi's method and simulated annealing cannot be used as self-optimizing algorithms because they need to perform network trials, i.e., test handover parameter settings, which is not possible in a real-time network. However, these two optimization methods are used in our context to benchmark the design of our proposed self-optimizing algorithm.

This paper is organized as follows. In Section II, the inter-RAT handover procedure comprising the handover-related parameters and the measurements leading to handover decisions are explained. The inter-RAT KPIs and their root-cause analysis are discussed in Section III. An overall description of the proposed self-optimizing algorithm for the inter-RAT LTE and 3G handover parameters is presented in Section IV. In Section V, we focus on describing in detail the two components of the feedback controller: the proportional control block and the gain scheduler. The simulation scenario and parameters for the LTE and 3G downlink systems are described in Section VI. Simulation results are shown in Section VII, and the performance of the proposed inter-RAT MRO algorithm is compared with those of three fixed handover parameter settings. In addition, the performance of the proposed algorithm is compared with those achieved by Taguchi's method and simulated annealing. This paper is then concluded in Section VIII.

II. INTER-RADIO ACCESS TECHNOLOGY HANDOVER PROCEDURE

Here, the inter-RAT handover measurements and parameters are explained after giving a few definitions.

A. General Definitions

- The RAT to which a cell c in LTE or 3G belongs is determined by the function $r = R(c)$, where r is either equal to LTE or 3G.
- Cell c serving user equipment (UE) u at time instant t is given by connection function $c = x_u(t)$.
- The downlink signal-to-interference-plus-noise ratio (SINR) of UE u served by cell c at time instant t is denoted by $\gamma_{u,c}(t)$.
- A radio link failure (RLF) is detected at time instant t_0 if the SINR of UE u falls below a certain threshold Q_{out} for a certain time interval $T_{Q_{\text{out}}}$, i.e.,

$$\gamma_{u,c}(t) < Q_{\text{out}} \text{ for } t_0 - T_{Q_{\text{out}}} < t < t_0. \quad (1)$$

B. Inter-RAT Handover Measurements and Parameters

The serving BS in LTE or 3G networks configures the UE to perform signal strength measurements for the serving and intra- or inter-RAT neighboring cells. The criteria for the UE to send its measurements in a report to the serving BS can be either periodic or event triggered. For an event triggered report, the UE sends its measurement report when a certain condition, which is called the entering condition of the measurement event, is fulfilled for a time-to-trigger (TTT) time interval denoted by T_T . The parameters of the entering condition of a measurement event are configured by the serving BS. The handover of the UE is triggered by the serving BS when a measurement report is received.

To hand over the UE from LTE to 3G, the serving BS in LTE configures the UE with measurement event B2 [26]. A similar measurement event exists for handing over the UE in a 3G cell to another LTE cell, which is called event 3A [27]. Both measurement events B2 and 3A require the UE to measure the received signal strength of both the serving and handover target cells. For an LTE cell, the UE measures the reference signal received power (RSRP), which is defined as the linear average over the power contributions of the resource elements that carry cell-specific reference signals within the considered measured frequency bandwidth [28]. In the case of a 3G cell, the UE measures the received signal code power (RSCP), which is defined as the received power on one code measured on the primary common pilot channel (CPICH) [28]. Both RSRP and RSCP include path loss, antenna gain, lognormal shadowing, and fast fading.

The received signal strength of serving cell c measured by UE u is expressed as a function of time t by $S_{u,c}(t)$ in dBm, i.e., $S_{u,c}(t)$ is equivalent to RSRP or RSCP if the UE is connected to LTE or 3G, respectively. Similarly, the signal strength of the handover target cell c_0 of UE u is expressed by $T_{u,c_0}(t)$ in dBm. Target cell c_0 is defined as the neighboring inter-RAT cell corresponding to the strongest signal strength measured and reported by UE u . The entering condition of measurement event B2 or 3A is fulfilled when the signal of the serving cell $S_{u,c}(t)$ falls below a first threshold S_{thr} expressed in dBm, and the signal of the target cell $T_{u,c_0}(t)$ is higher than a second threshold T_{thr} in dBm. The UE sends the measurement report at

time instant t_0 when the entering condition of the measurement event is fulfilled for a time interval of T_T duration, i.e.,

$$S_{u,c}(t) < S_{\text{thr}} \wedge T_{u,c_0}(t) > T_{\text{thr}} \text{ for } t_0 - T_T < t < t_0 \\ \text{such that } R(c) \neq R(c_0). \quad (2)$$

In principle, the UE starts to measure the neighboring inter-RAT cells when the signal strength of the serving cell falls below a certain network-configured threshold. The latter threshold would be set slightly above S_{thr} , so that $T_{u,c_0}(t)$ would be available when the UE checks if the entering condition of the measurement event is fulfilled. In this paper, we assume for simplicity that the inter-RAT measurements are always available for the UE. It is also worth noting that, to measure the signal strength of neighboring inter-RAT cells, the UE has to interrupt its serving connection for measurement gaps [29]. From that perspective, inter-RAT measurements are quite costly, unlike the intra-RAT case, which does not require any measurement gaps.

The two thresholds S_{thr} and T_{thr} are called inter-RAT handover thresholds, and these shall be optimized by the inter-RAT MRO algorithm, assuming that T_T is configured properly. Large T_T values can avoid handovers caused by measurement outliers; however, they may delay the handover decisions that may lead to RLFs, particularly for fast UEs. Extending the inter-RAT MRO algorithm to comprise T_T optimization is left for future work.

C. Execution of the Inter-RAT Handover

After a measurement report is sent by UE u , serving cell c prepares the handover of the UE by sending a handover request to target handover cell c_0 . Then, serving cell c waits for an acknowledgment from target cell c_0 . This step induces an additional delay T_{HP} , which we typically call handover preparation time. Therefore, the handover of UE u is executed T_{HP} s after the measurement event is triggered as long as the SINR $\gamma_{u,c}(t)$ of the UE is greater than threshold Q_{fail} . In other words, the handover of UE u is executed from cell c to cell c_0 at time instant t_{HO} if the following conditions hold:

$$x_u(t) = c_0 \text{ for } t > t_{\text{HO}} \\ \text{if } S_{u,c}(t) < S_{\text{thr}} \wedge T_{u,c_0}(t) > T_{\text{thr}} \\ \text{for } t_{\text{HO}} - T_{\text{HP}} - T_T < t < t_{\text{HO}} - T_{\text{HP}}, \\ R(c) \neq R(c_0), \text{ and } \gamma_{u,c}(t_{\text{HO}}) > Q_{\text{fail}}. \quad (3)$$

Connection function $x_u(t)$ is changed to c_0 at time instance t_{HO} until the succeeding handover is executed.

III. KPIS FOR INTER-RADIO ACCESS TECHNOLOGY MOBILITY PERFORMANCE

Here, the inter-RAT mobility KPIS and the root-cause analysis of each type of mobility failure events are presented. The more detailed the information about the mobility failure events, the better the optimization algorithm is. In accordance with the mobility failure types defined for the intra-LTE case [5], two categories are specified here for the inter-RAT scenario:

The first category captures inter-RAT RLFs and the second category captures the costly inter-RAT handovers, such as ping-pongs (PPs), which refer to events where the UE is immediately handed back over to a cell of its previous RAT after a successful inter-RAT handover.

A. Inter-RAT RLF KPIS

There are three types of RLF mobility events: 1) a too-late inter-RAT handover (TLH); 2) a too-early inter-RAT handover (TEH); and 3) an inter-RAT handover to a wrong cell (HWC).

1) *TLH*: The UE drops before a handover is initiated or executed from one RAT to another, and the UE reconnects to a cell in a RAT, which is different than that of the previously serving cell. The reason for a TLH is either the entering condition of the measurement event had not been fulfilled or the entering condition of the measurement event had been fulfilled, but the RLF occurred before the inter-RAT handover is executed.

The entering condition of a measurement event is not fulfilled in three different cases.

- Case A: $S_{u,c}(t)$ is below S_{thr} and $T_{u,c_0}(t)$ is below T_{thr} [see Fig. 1(a)].
- Case B: $S_{u,c}(t)$ is higher than S_{thr} and $T_{u,c_0}(t)$ is higher than T_{thr} [see Fig. 1(b)].
- Case C: $S_{u,c}(t)$ is higher than S_{thr} and $T_{u,c_0}(t)$ is below T_{thr} [see Fig. 1(c)].

In another case, denoted as Case D and shown in Fig. 1(d), the entering condition of the measurement event is fulfilled, but nevertheless, the RLF occurred before the inter-RAT handover is completed.

In an intra-RAT case, a single handover threshold is used, and consequently, one type of TLH exists. However, in an inter-RAT case, there are two thresholds controlling each measurement event B2 and 3A, and the root cause for a TLH is the misconfiguration of either S_{thr} or T_{thr} . A TLH due to the misconfiguration of S_{thr} or T_{thr} is denoted by $\text{TLH}(S_{\text{thr}})$ or $\text{TLH}(T_{\text{thr}})$, respectively. Our proposal to distinguish between the two types $\text{TLH}(S_{\text{thr}})$ and $\text{TLH}(T_{\text{thr}})$ has been recently adopted by LTE Release 11 (Rel. 11) standard [30], [31]. In Case A, the entering condition of the measurement event is not fulfilled because T_{thr} is set to a too high value, which cannot be achieved, i.e., the RLF occurred before $T_{u,c_0}(t)$ becomes higher than T_{thr} . In this case, the misconfiguration of T_{thr} is the root cause for the TLH. Similarly, in Case B, the entering condition of the measurement event is not fulfilled because S_{thr} is set to a too low value, and the RLF occurred before $S_{u,c}(t)$ becomes lower than S_{thr} . In this case, the misconfiguration of S_{thr} is the root cause for the TLH.

For Cases C and D, the root cause for the TLH is not as obvious as in Cases A and B. In Case C, none of the two thresholds is reached, i.e., $S_{u,c}(t) > S_{\text{thr}}$ and $T_{u,c_0}(t) < T_{\text{thr}}$, and in Case D, both thresholds are reached, i.e., $S_{u,c}(t) < S_{\text{thr}}$ and $T_{u,c_0}(t) > T_{\text{thr}}$. In Case C, the root cause for the TLH is, in principle, the misconfiguration of both S_{thr} and T_{thr} thresholds because they are not reached. However, as each TLH should be counted as a single mobility failure event, it has to be classified as either $\text{TLH}(S_{\text{thr}})$ or $\text{TLH}(T_{\text{thr}})$. For this purpose, we propose a new classification rule that is based

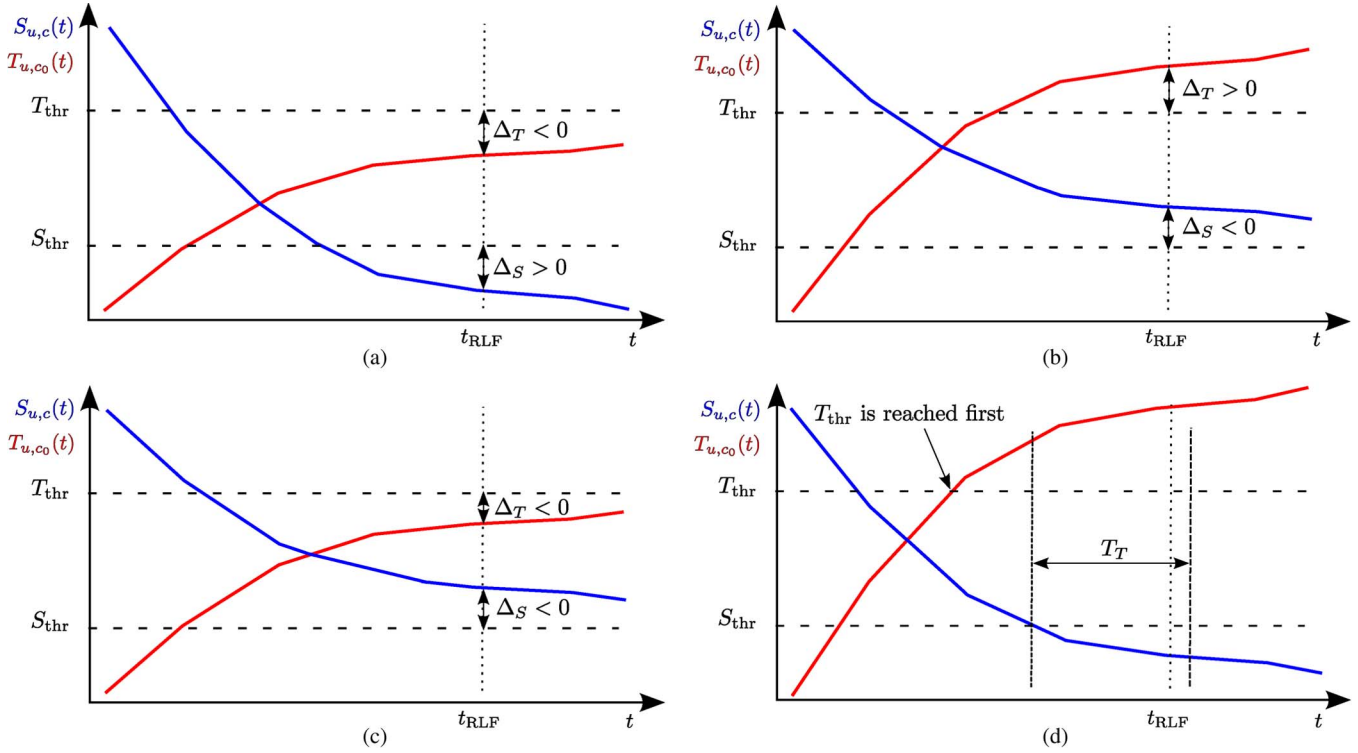


Fig. 1. Four different cases for inter-RAT TLH. (a) Case A where the entering condition of the measurement event is not fulfilled. The misconfiguration of T_{thr} is the root cause for the TLH. (b) Case B where the entering condition of the measurement event is not fulfilled. The misconfiguration of S_{thr} is the root cause for the TLH. (c) Case C where the entering condition of the measurement event is not fulfilled. The misconfiguration of the threshold corresponding to the smallest value between Δ_S and Δ_T is identified as the root cause for the TLH. (d) Case D where the entering condition of the measurement event is fulfilled. The misconfiguration of one of the two thresholds, which is reached later, is identified as the root cause for the TLH.

on the differences between the values of the thresholds and their corresponding measured signal levels evaluated at t_{RLF} . Let $\Delta_S = S_{thr} - S_{u,c}(t_{RLF})$ and $\Delta_T = T_{u,c_0}(t_{RLF}) - T_{thr}$ be the differences corresponding to thresholds S_{thr} and T_{thr} , respectively. The root cause for the TLH in Case C is identified as the misconfiguration of the threshold of which the difference is the smallest. The rule determines the threshold that has to be adjusted first by comparing the two negative values Δ_S and Δ_T . Once the threshold corresponding to the smallest difference is correctly adjusted in subsequent steps, i.e., its corresponding value of Δ_S or Δ_T becomes positive, the rule detects that the other threshold having $\Delta_S < 0$ or $\Delta_T < 0$ has to be adjusted. As a result, the rule needs multiple steps to detect that both thresholds have to be adjusted and consequently resolve the TLH. The proposed routine for classifying a TLH as either $TLH(S_{thr})$ or $TLH(T_{thr})$ in Cases A, B, and C is summarized in pseudocode 1.

Pseudocode 1: Routine for classifying a TLH as either $TLH(S_{thr})$ or $TLH(T_{thr})$.

- 1: Input Parameters: $S_{u,c}(t_{RLF})$, $T_{u,c_0}(t_{RLF})$, S_{thr} , and T_{thr} .
- 2: Calculate $\Delta_S = S_{thr} - S_{u,c}(t_{RLF})$.
- 3: Calculate $\Delta_T = T_{u,c_0}(t_{RLF}) - T_{thr}$.
- 4: **if** $\Delta_S < \Delta_T$
- 5: TLH is classified as $TLH(S_{thr})$.
- 6: **else**

7: TLH is classified as $TLH(T_{thr})$.

8: **end if**

As for Case D, the root cause for the TLH cannot be determined using the aforementioned pseudocode. In this case, the root cause for the TLH is the misconfiguration of one of the two thresholds, which is reached later. For clarity, an example is shown in Fig. 1(d), which shows Case D. According to the figure, the entering condition of the measurement event is fulfilled; nevertheless, an RLF occurred before the T_T time interval is completed. The TLH could be resolved if the entering condition would have been fulfilled earlier. To this end, the threshold that delayed the fulfillment of the entering condition needs to be determined and adjusted. In this example, T_{thr} is reached before S_{thr} , and the root cause for this RLF is the misconfiguration of S_{thr} . Decreasing T_{thr} would not solve the TLH as the entering condition would not be fulfilled earlier since $S_{u,c}(t)$ is greater than S_{thr} . However, if S_{thr} is reached earlier, the entering condition of the measurement event would have been fulfilled earlier, and the RLF would have been avoided. We note that to resolve $TLH(S_{thr})$, S_{thr} should be increased, whereas $TLH(T_{thr})$ is resolved by decreasing the T_{thr} threshold.

2) *TEH*: The UE is successfully handed over from cell A to another cell B of a different RAT. Shortly after, an RLF happens, and the UE reconnects to the previous RAT, either to the same cell A or to a different one. Moreover, the inter-RAT handover failure, occurring when the UE fails during the

handover to connect to the target handover cell c_0 using the random access channel [32], is also considered a TEH. The root cause for a TEH is the misconfiguration of T_{thr} , which should be increased to guarantee that the signal of the target cell of a different RAT is strong enough.

3) *HWC*: The UE is successfully handed over from cell A to another cell B of a different RAT. Shortly after, an RLF happens, and the UE reconnects to a third cell C belonging to the same RAT as cell B. Similar to a TEH, the root cause for a HWC is the misconfiguration of T_{thr} , which should be increased to guarantee that the signal of a cell of a different RAT is strong enough.

B. Costly Inter-RAT Handovers

There are two types of costly inter-RAT handovers: Inter-RAT PPs and unnecessary handovers (UHs) from LTE to 3G. The number of UHs has to be minimized as the users should benefit as much as possible from the newly deployed LTE network, which is given, in our case, a higher priority than 3G.

1) *PP*: The UE is handed over to a cell of a different RAT, and within time interval T_{PP} , the UE is handed over back to the same cell or to a different cell of the previous RAT. The action needed to resolve a PP is to delay the first inter-RAT handover by either decreasing S_{thr} or increasing T_{thr} .

2) *UH*: The UE is handed over from a high-priority RAT (LTE in our case) to a low priority RAT (3G), although the signal quality of the previous LTE cell is still good enough [32]. In this paper, an inter-RAT handover is detected as unnecessary if, after the handover, the reference signal received quality (RSRQ) of the previous LTE cell is still higher than threshold Q_{RSRQ} for time interval $T_{Q_{RSRQ}}$. The action needed to resolve UHs is to increase the coverage of the LTE cell by decreasing S_{thr} .

In this paper, we consider all types of mobility failures and costly handovers for the inter-RAT scenario. However, in practice, the Third-Generation Partnership Project has focused only on a subset of the aforementioned KPIs. The LTE Rel. 10 standard has specified the detection of UHs, whereas LTE Rel. 11 has recently considered TLHs from LTE to 3G, TEHs from 3G to LTE, and PPs in both RATs [32].

IV. DESCRIPTION OF THE SELF-OPTIMIZING ALGORITHM FOR INTER-RADIO ACCESS TECHNOLOGY HANDOVER-RELATED PARAMETERS

Here, we give a general overview of the proposed inter-RAT MRO algorithm. Some of the inter-RAT KPIs defined in Section III require the same action to be performed on the value of a handover threshold, i.e., either increase or decrease. Therefore, we group the values of the inter-RAT KPIs into new other values depending on the action that needs to be applied on each handover threshold. The feedback controller determines the change in the magnitude of each handover threshold based on the aforementioned new values.

A. Grouping the Values of the Inter-RAT KPIs

The optimization loop for the inter-RAT handover thresholds, as shown in Fig. 2, is carried out per LTE and 3G cell indepen-

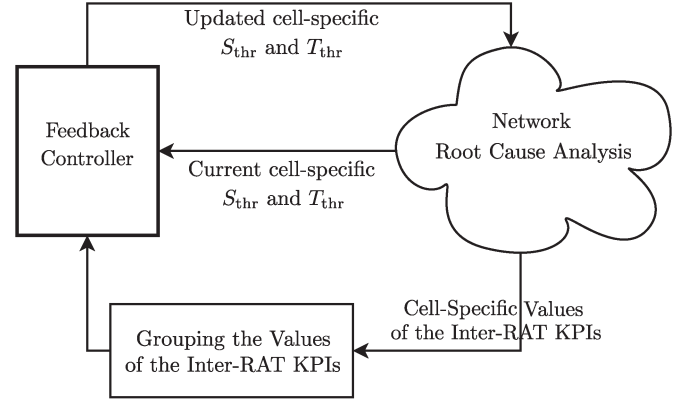


Fig. 2. Description of the optimization loop for the inter-RAT handover thresholds.

dently, i.e., both LTE and 3G cells apply the same kind of an optimization algorithm and loop. The joint optimization of the handover thresholds of all LTE and 3G cells in a distributed way is currently impractical as it requires the standardization of additional signaling messages between the BSs, particularly if they are from different manufacturing vendors. Moreover, the advantage of independently optimizing the handover thresholds of each cell is that it does not incur any signaling overhead compared with the joint optimization.

The mobility failure event of UE is counted by the responsible cell of which the misconfiguration of its handover threshold is the root cause for that failure. The values of the inter-RAT KPIs are collected in the responsible cell during the root-cause analysis period of duration T_{KPI} . We denote the values of TLH(S_{thr}), TLH(T_{thr}), TEH, HWC, PP, and UH collected in KPI period k by $N_{TLH-S}^{(k)}$, $N_{TLH-T}^{(k)}$, $N_{TEH}^{(k)}$, $N_{HWC}^{(k)}$, $N_{PP}^{(k)}$, and $N_{UH}^{(k)}$, respectively. In each KPI period k , new values of KPIs are collected per cell. In this paper, the values of the KPIs are cell-specific and not cell-pair specific, i.e., the mobility failure events are not differentiated with respect to each handover target cell. This is because the two inter-RAT handover thresholds used by LTE and 3G cells are cell-specific thresholds [26], [27]. In the future study, we will investigate whether the additional complexity incurred by the cell-pair specific optimization can be justified by the expected gain in performance compared with cell-specific optimization. The two handover thresholds applied by a cell in KPI period k are denoted by $S_{thr}^{(k)}$ and $T_{thr}^{(k)}$.

After the root-cause analysis period, the collection of cell-specific values of KPIs is stopped. Then, each cell groups the values of its KPIs into four new values, which are denoted by group values, and defined as follows: $S_k^{(+)}$ and $S_k^{(-)}$ are the numbers of mobility failure events in KPI period k that require an increase and a decrease, respectively, in $S_{thr}^{(k)}$, and $T_k^{(+)}$ and $T_k^{(-)}$ are the numbers of mobility failure events in KPI period k that require an increase and a decrease, respectively, in $T_{thr}^{(k)}$. The values of the KPIs are grouped to one of the four aforementioned new values, as shown in Fig. 3. In the case of a 3G cell, the value $N_{UH}^{(k)}$ of the UH KPI does not exist and is excluded from the grouping.

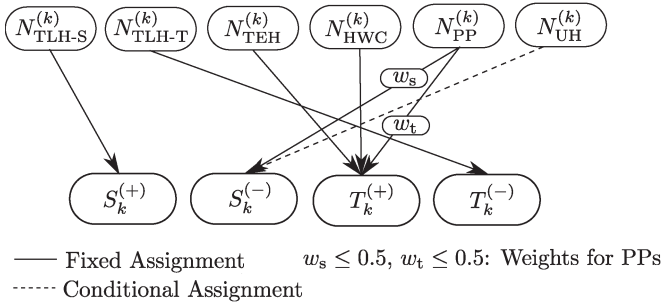


Fig. 3. Grouping the values of the KPIs into four new values based on the actions required for updating the handover thresholds. In the case of a 3G cell, $N_{UH}^{(k)}$ does not exist and is excluded.

The main aim of the inter-RAT MRO algorithm is to resolve RLFs and high $N_{PP}^{(k)}$ might prevent the algorithm from reacting on $N_{TLH-S}^{(k)}$ and $N_{TLH-T}^{(k)}$. To overcome this problem, $N_{PP}^{(k)}$ is weighted by coefficients $w_s \leq 0.5$ and $w_t \leq 0.5$ to give a higher priority for RLFs. In this case, each PP event is counted $(w_s + w_t) \leq 1$ times compared with an RLF event, which is counted once. For instance, if a weight of 0.2 is used for w_s and w_t , a PP event is counted $(w_s + w_t) = 0.4$ times compared with an RLF event. The higher the values of w_s and w_t , the higher the probability of reducing the gains in RLFs is. Moreover, among the assignments, there is one which is conditional: $N_{UH}^{(k)}$ is assigned to $S_k^{(-)}$ only when there is no TLHs in the cell. The coverage of the LTE cell should be increased only if the UE could continue in the source cell without problems, as stated in the LTE standard [33]. The existence of TLHs is an indication that the UE could not stay longer in the cell and should be handed over earlier. As a result, reacting on UHs with the presence of TLHs is risky and may worsen the mobility performance of the UE. Having the values of the KPIs grouped, the four aforementioned group values are used by the feedback controller to update the handover thresholds $S_{thr}^{(k)}$ and $T_{thr}^{(k)}$ of KPI period k .

B. Description of the Feedback Controller

Here, we give a general overview of the feedback controller, which is responsible for updating the handover thresholds $S_{thr}^{(k)}$ and $T_{thr}^{(k)}$.

In KPI period k , the input variables of the controller are the four group values $S_k^{(+)}$, $S_k^{(-)}$, $T_k^{(+)}$, and $T_k^{(-)}$ obtained from grouping the values of the KPIs in addition to the values of the thresholds $S_{thr}^{(k-1)}$ and $T_{thr}^{(k-1)}$ used in KPI period $k-1$ (see Fig. 2). The changes in the magnitude of thresholds $S_{thr}^{(k)}$ and $T_{thr}^{(k)}$ are denoted by $u_{s,dB}^{(k)}$ and $u_{t,dB}^{(k)}$, which are expressed in decibels, respectively. The role of the feedback controller is to determine the appropriate values of $u_{s,dB}^{(k)}$ and $u_{t,dB}^{(k)}$ based on the input variables fed to the controller in each KPI period.

Threshold $S_{thr}^{(k)}$ is increased or decreased by $u_{s,dB}^{(k)}$ only if one or both group values $S_k^{(+)}$ and $S_k^{(-)}$ exceed a certain limit denoted by $S^{(min)}$. Similarly, $T_{thr}^{(k)}$ is updated if one or both $T_k^{(+)}$ and $T_k^{(-)}$ exceed a predefined limit denoted by $T^{(min)}$. The

values of $S^{(min)}$ and $T^{(min)}$ depend mainly on the duration of the KPI collection period and the number of handover attempts in the cell, i.e., too-late handovers + successful handovers. Thresholds $S^{(min)}$ and $T^{(min)}$ should be set high enough, so that the group values can be considered statistically significant and in turn avoid reacting on outliers.

The value of $u_{s,dB}^{(k)}$ is determined based on the magnitude of $S_k^{(+)}$ and $S_k^{(-)}$. Similarly, the value of $u_{t,dB}^{(k)}$ is determined based on the magnitude of $T_k^{(+)}$ and $T_k^{(-)}$. The value of $u_{s,dB}^{(k)}$ depends on the difference between $S_k^{(+)}$ and $S_k^{(-)}$, as shown in Fig. 4. The same applies for $u_{t,dB}^{(k)}$. The larger the difference between $S_k^{(+)}$ and $S_k^{(-)}$, the larger $u_{s,dB}^{(k)}$ is. If the difference between $S_k^{(+)}$ and $S_k^{(-)}$ is significant, as in Fig. 4(a), large $u_{s,dB}^{(k)}$ is used since one specific value is dominating and can be well reduced. However, it may happen that two similar group values occur in one cell, as shown in Fig. 4(c). In this case, the mobility failure events require contradicting handover threshold updates. Changing the threshold in one direction could decrease one of the group values more than the other one is increased; however, it would be difficult to predict the correct parameter update, i.e., increase or decrease. Moreover, the gain would be minimal if it exists since none of the group values can be well reduced without a significant increase in the other group value, i.e., the group values would most likely start to oscillate. Reducing the oscillations in the values of the KPIs is an important aspect in self-optimizing algorithms as they directly impact the quality perception of the users. Therefore, in this case, we either apply small $u_{s,dB}^{(k)}$ or avoid updating the handover threshold, i.e., $u_{s,dB}^{(k)} = 0$.

The problem shown in Fig. 4(c) can be tackled for the target threshold using cell-pair specific handover offsets, which allow a *dedicated* handover threshold value to be configured with respect to each neighboring target cell. For clarity, assume that $T_k^{(+)} \approx T_k^{(-)}$ and the mobility failure events of $T_k^{(+)}$ occur with respect to neighboring target cell c'_0 , which is different than that of $T_k^{(-)}$ denoted by c''_0 . By means of cell-pair specific handover thresholds, the target threshold could be increased with respect to c'_0 and decreased with respect to c''_0 , which consequently resolve $T_k^{(+)}$ and $T_k^{(-)}$. This solution is currently not possible since the inter-RAT handover thresholds are specified as cell-specific.

V. COMPONENTS OF THE CONTROLLER

The feedback controller, highlighted in bold in Fig. 2, is composed of two components: a proportional control block and a gain scheduler, as shown in Fig. 5. The input variables to the feedback controller are the four group values and the handover threshold values of KPI period $k-1$ and the output is the updated handover thresholds of KPI period k .

A. Proportional Control Block

1) *Calculate the Error Values*: We define two metrics $M_s^{(k)}$ and $M_t^{(k)}$ corresponding to handover thresholds $S_{thr}^{(k)}$ and $T_{thr}^{(k)}$,

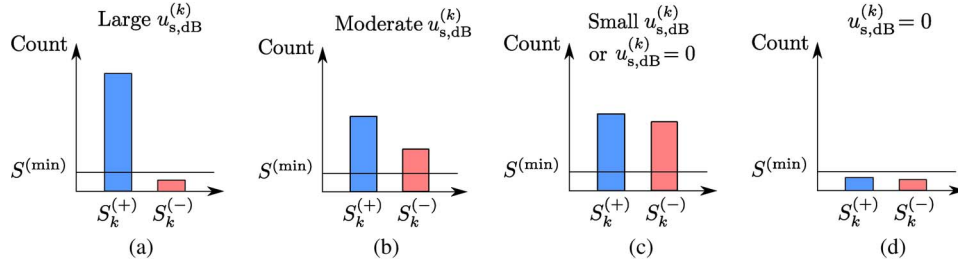


Fig. 4. Value of $u_{s,dB}^{(k)}$ depends on the difference between $S_k^{(+)}$ and $S_k^{(-)}$. The same applies for $u_{t,dB}^{(k)}$. (a) Large $u_{s,dB}^{(k)}$ is applied if the difference between $S_k^{(+)}$ and $S_k^{(-)}$ is large. (b) Moderate $u_{s,dB}^{(k)}$ is applied if the difference between $S_k^{(+)}$ and $S_k^{(-)}$ is moderate. (c) Small $u_{s,dB}^{(k)}$ or $u_{s,dB}^{(k)} = 0$ is applied if the difference between $S_k^{(+)}$ and $S_k^{(-)}$ is small. (d) $u_{s,dB}^{(k)} = 0$ is applied if $S_k^{(+)}$ and $S_k^{(-)}$ are below $S^{(min)}$.

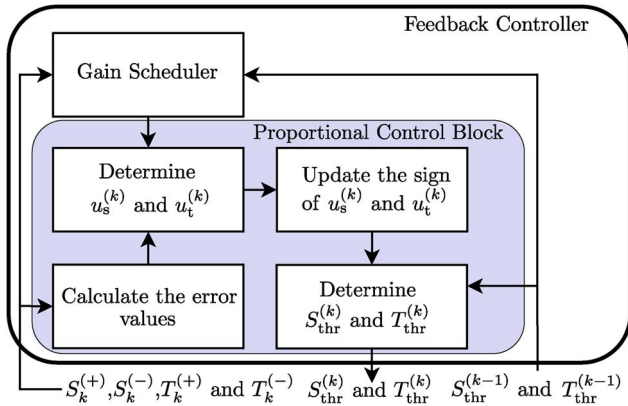


Fig. 5. Description of the feedback controller consisting of a proportional control block and a gain scheduler.

respectively, as follows:

$$M_s^{(k)} = \frac{\max \{S_k^{(+)}, S_k^{(-)}\}}{\min \{S_k^{(+)}, S_k^{(-)}\}} \geq 1, \quad (4)$$

$$M_t^{(k)} = \frac{\max \{T_k^{(+)}, T_k^{(-)}\}}{\min \{T_k^{(+)}, T_k^{(-)}\}} \geq 1. \quad (5)$$

The larger $M_s^{(k)}$ or $M_t^{(k)}$, the larger $u_{s,dB}^{(k)}$ or $u_{t,dB}^{(k)}$ is, respectively. In contrast, a small $M_s^{(k)}$ requires a small $u_{s,dB}^{(k)}$. The proportional control block makes corrective actions based on the value of an error, which is defined in our case as a function of the aforementioned metric. The higher the error value, the larger the change in the magnitude of a handover threshold value is. The handover threshold is not updated when the error is equal to zero, which occurs when both group values are below a certain limit or they are equal to each other, e.g., $M_s^{(k)} = 1$. Therefore, we define the error values $e_s^{(k)}$ and $e_t^{(k)}$ as follows:

$$e_s^{(k)} = \begin{cases} M_s^{(k)} - 1 \geq 0, & \text{if } S_k^{(+)} \text{ or } S_k^{(-)} > S^{(min)} \\ 0, & \text{otherwise} \end{cases} \quad (6)$$

$$\text{and } e_t^{(k)} = \begin{cases} M_t^{(k)} - 1 \geq 0, & \text{if } T_k^{(+)} \text{ or } T_k^{(-)} > T^{(min)} \\ 0, & \text{otherwise.} \end{cases} \quad (7)$$

The aim of the controller is to minimize these error values.

2) *Determine $u_{s,dB}^{(k)}$ and $u_{t,dB}^{(k)}$* : Many models exist for expressing $u_{s,dB}^{(k)}$ and $u_{t,dB}^{(k)}$ as a function of the errors $e_s^{(k)}$ and $e_t^{(k)}$, respectively. One simple model is to express $u_{s,dB}^{(k)}$ as a linear function of $e_s^{(k)}$. In other words, the value of $u_{s,dB}^{(k)}$ is proportional to the error $e_s^{(k)}$. To this end, let $u_{s,dB}^{(k,max)}$ and $u_{t,dB}^{(k,max)}$ be the maximum predefined changes in the magnitude that can be applied to $S_{thr}^{(k)}$ and $T_{thr}^{(k)}$ in KPI period k , respectively. Parameters $u_{s,dB}^{(k,max)}$ and $u_{t,dB}^{(k,max)}$ are applied when the error values $e_s^{(k)}$ and $e_t^{(k)}$ exceed the maximum predefined error values $e_s^{(max)}$ and $e_t^{(max)}$, respectively. The values of $u_{s,dB}^{(k)}$ and $u_{t,dB}^{(k)}$ are calculated as follows:

$$u_{s,dB}^{(k)} = \begin{cases} u_{s,dB}^{(k,max)}, & \text{if } e_s^{(k)} \geq e_s^{(max)} \\ K_s^{(k)} \cdot e_s^{(k)}, & \text{if } 0 \leq e_s^{(k)} < e_s^{(max)} \end{cases} \quad (8)$$

$$u_{t,dB}^{(k)} = \begin{cases} u_{t,dB}^{(k,max)}, & \text{if } e_t^{(k)} \geq e_t^{(max)} \\ K_t^{(k)} \cdot e_t^{(k)}, & \text{if } 0 \leq e_t^{(k)} < e_t^{(max)} \end{cases} \quad (9)$$

where the controller gains $K_s^{(1)}$ and $K_t^{(1)}$ are equal to $u_{s,dB}^{(1,max)} / e_s^{(max)}$ and $u_{t,dB}^{(1,max)} / e_t^{(max)}$, respectively, in the first KPI period, i.e., $k = 1$. The values of the controller gains $K_s^{(k)}$ and $K_t^{(k)}$, and $u_{s,dB}^{(k,max)}$ and $u_{t,dB}^{(k,max)}$ are updated by the gain scheduler to reduce the oscillations in the system (see Section V-B). In the context of control theory, the interval $(0, e_s^{(max)})$ or $(0, e_t^{(max)})$ is called the proportional band because the behavior of the controller is linear when the error lies in these intervals. For clarity, the unquantized value of $u_{s,dB}^{(k)}$ is shown in Fig. 6 as a function of error $e_s^{(k)}$ for $e_s^{(max)} = 1.5$ and different values for pair $(K_s^{(k)}, u_{s,dB}^{(k,max)})$.

3) *Update the Sign of $u_{s,dB}^{(k)}$ and $u_{t,dB}^{(k)}$* : The sign of $u_{s,dB}^{(k)}$ depends on whether $S_k^{(+)}$ is greater than $S_k^{(-)}$ or vice versa. The same applies for $u_{t,dB}^{(k)}$. The values of $u_{s,dB}^{(k)}$ and $u_{t,dB}^{(k)}$ are updated as follows:

$$u_{s,dB}^{(k)} = \begin{cases} u_{s,dB}^{(k)}, & \text{if } S_k^{(+)} > S_k^{(-)} \\ -u_{s,dB}^{(k)}, & \text{if } S_k^{(+)} < S_k^{(-)} \end{cases} \quad (10)$$

$$u_{t,dB}^{(k)} = \begin{cases} u_{t,dB}^{(k)}, & \text{if } T_k^{(+)} > T_k^{(-)} \\ -u_{t,dB}^{(k)}, & \text{if } T_k^{(+)} < T_k^{(-)}. \end{cases} \quad (11)$$

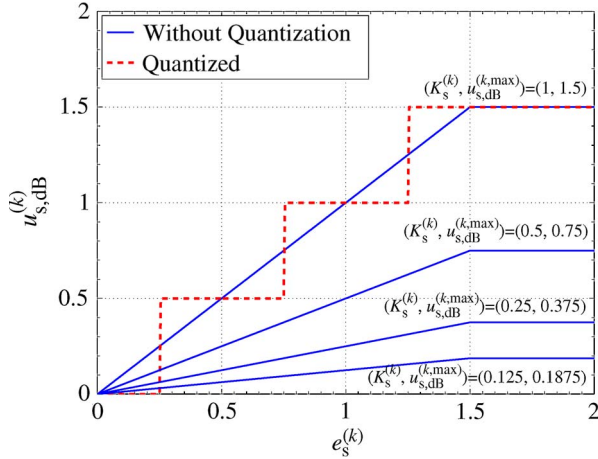


Fig. 6. Value of $u_{s,dB}^{(k)}$ as a function of the error $e_s^{(k)}$ for $e_s^{(max)} = 1.5$ and different values for pair $(K_s^{(k)}, u_{s,dB}^{(k,max)})$.

4) *Determine $S_{thr}^{(k)}$ and $T_{thr}^{(k)}$* : The updated threshold values $S_{thr}^{(k)}$ and $T_{thr}^{(k)}$ are signaled to the UE via measurement configuration messages. To reduce the signaling overhead, the number of changes in the magnitude of the handover thresholds is limited by quantizing $u_{s,dB}^{(k)}$ and $u_{t,dB}^{(k)}$ with quantization step sizes $\lambda_{s,dB}$ and $\lambda_{t,dB}$, respectively. An example is depicted in Fig. 6, which shows the quantized value of $u_{s,dB}^{(k)}$ with $\lambda_{s,dB} = 0.5$. The quantized values of $u_{s,dB}^{(k)}$ and $u_{t,dB}^{(k)}$ are denoted by $Q_{s,dB}^{(k)}$ and $Q_{t,dB}^{(k)}$, respectively. The values of $S_{thr}^{(k)}$ and $T_{thr}^{(k)}$ are finally updated as follows:

$$S_{thr}^{(k)} = S_{thr}^{(k-1)} + Q_{s,dB}^{(k)}, \quad (12)$$

$$T_{thr}^{(k)} = T_{thr}^{(k-1)} + Q_{t,dB}^{(k)}. \quad (13)$$

The values of $S_{thr}^{(k)}$ and $T_{thr}^{(k)}$ are fed into the network and the process is repeated.

B. Gain Scheduler

The gain scheduler updates the parameters of the proportional control block depending on the mobility conditions in each cell.

1) *Reducing the Values of the Control Parameters*: With the proportional control block, a cell achieves stability when the group values are either of similar or equal magnitude, as shown in Fig. 4(c), or lower than the thresholds $S^{(min)}$ and $T^{(min)}$, as in Fig. 4(d). In both cases, no handover threshold update is performed, i.e., $u_{s,dB}^{(k)} = 0$, and $u_{t,dB}^{(k)} = 0$. However, the cell may not always reach one of the latter two stable cases. For instance, it may happen that reducing $S_k^{(+)}$ leads to a large increase in $S_k^{(-)}$ and *vice versa*. In this case, $S_k^{(+)}$ and $S_k^{(-)}$ oscillate with each handover threshold update. One example of an oscillation in the group values is shown in Fig. 7. In KPI period $k-2$, $S_{k-2}^{(+)} > S_{k-2}^{(-)}$, and the threshold S_{thr} is increased accordingly. The increase in S_{thr} has caused an increase in $S_{k-1}^{(-)}$ in KPI period $k-1$. Threshold S_{thr} is then decreased. In KPI period k , the decrease in S_{thr} has caused again an increase

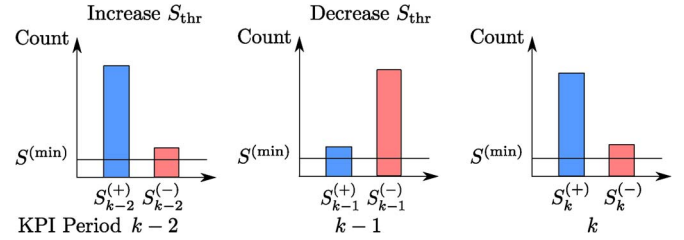


Fig. 7. Example of an oscillation in the group values detected in KPI period k .

in $S_k^{(+)}$ and a decrease in $S_k^{(-)}$. In this case, an oscillation in the group values is detected. Therefore, in this situation, the thresholds are constantly updated up and down, and stability is not reached.

The role of the gain scheduler is to modify the control parameters of the proportional control block depending on the mobility conditions in each cell, which are identified by the observable variables or so-called scheduling variables in the vocabulary of control theory [15]. The first observable variable used by the gain scheduler is a boolean flag indicating if an oscillation in the group values occurred, as shown in Fig. 7. Once an oscillation in the group values is detected, the gain scheduler reduces the controller gains $K_s^{(k)}$ and $K_t^{(k)}$ by the reduction ratios $\rho_s < 1$ and $\rho_t < 1$, respectively, as follows:

$$K_s^{(k)} = \rho_s \cdot K_s^{(k-1)}, \quad (14)$$

$$K_t^{(k)} = \rho_t \cdot K_t^{(k-1)}. \quad (15)$$

As a result, the gain scheduler modifies the behavior of the proportional control block with every oscillation in the group values. Decreasing the controller gain $K_s^{(k)}$ by ρ_s leads to a reduction in the value of $u_{s,dB}^{(k)}$ by a factor of ρ_s if the error $e_s^{(k)}$ lies within the proportional band [see (8)]. Therefore, the value of $u_{s,dB}^{(k)}$ is reduced each time an oscillation is detected. If the number of oscillations is large, the value of $u_{s,dB}^{(k)}$ approaches 0, and stability is achieved. Keeping the error values $e_s^{(max)}$ and $e_t^{(max)}$ fixed, the values of $u_{s,dB}^{(k,max)}$ and $u_{t,dB}^{(k,max)}$ are updated as follows:

$$u_{s,dB}^{(k,max)} = K_s^{(k)} \cdot e_s^{(max)}, \quad (16)$$

$$u_{t,dB}^{(k,max)} = K_t^{(k)} \cdot e_t^{(max)}. \quad (17)$$

For instance, in Fig. 6, the value of $u_{s,dB}^{(k)}$ is plotted as a function of error $e_s^{(k)}$ with $K_s^{(k)}$ and $u_{s,dB}^{(k,max)}$ as parameters. Initially, $(K_s^{(k)}, u_{s,dB}^{(k,max)}) = (1, 1.5)$ is used. Once an oscillation is detected in $S_k^{(+)}$ and $S_k^{(-)}$, the gain scheduler reduces $(K_s^{(k)}, u_{s,dB}^{(k,max)})$ by $\rho_s = 0.5$, resulting in $(K_s^{(k)}, u_{s,dB}^{(k,max)}) = (0.5, 0.75)$ curve. If two additional oscillations are detected, $(K_s^{(k)}, u_{s,dB}^{(k,max)})$ are further reduced, resulting in $(K_s^{(k)}, u_{s,dB}^{(k,max)}) = (0.125, 0.1875)$. In this case, the value of $u_{s,dB}^{(k)}$ is lower than 0.25 for all error values; if quantization is considered with $\lambda_{s,dB} = 0.5$, $Q_{s,dB}^{(k)} = 0$ is used for all values of $e_s^{(k)}$, and stability is achieved.

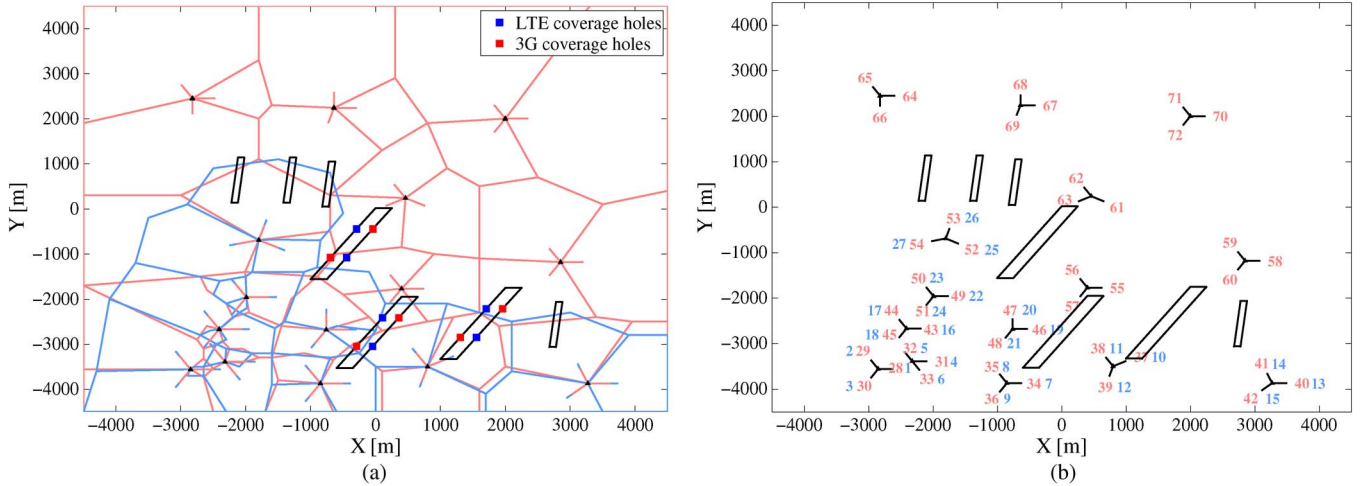


Fig. 8. Simulation scenario used to evaluate the performance of the inter-RAT MRO algorithm. (a) LTE network (blue) overlays 3G network (red). The seven street loops are shown in black. (b) ID numbers 1–27 are used for LTE cells (blue) and 28–72 for 3G cells (red).

2) *Increasing the Values of the Control Parameters:* A cell that has reduced $K_s^{(k)}$ or $K_t^{(k)}$ due to a series of oscillations may have to increase them again to react on any new changes in mobility failure events in the network, e.g., caused by changes in the environment or mobility conditions of the cell. For example, if one of the two group values requiring contradicting changes in the handover threshold has increased or decreased significantly, the inter-RAT MRO algorithm should be able to react again. Therefore, there should be a procedure to escape from small values of $K_s^{(k)}$ or $K_t^{(k)}$ in the case of an abrupt change in the group values of the considered cell. For instance, let $\delta_s^{(k)}$ be the change in the magnitude of $S_k^{(+)}$ in KPI period k . $\delta_s^{(k)}$ is defined as the minimum distance between $S_k^{(+)}$ and its corresponding $n_s \geq 1$ previous values, i.e.,

$$\delta_s^{(k)} = \min_{i=1, \dots, n_s} |S_k^{(+)} - S_{k-i}^{(+)}|. \quad (18)$$

Parameter n_s is introduced to guarantee that the change $\delta_s^{(k)}$ in $S_k^{(+)}$ is not due to a statistical fluctuation, i.e., $S_k^{(+)}$ might vary in each KPI period even if $S_{thr}^{(k)}$ is not changed. Variable $\delta_s^{(k)}$ is the second observable variable used by the gain scheduler. If the value of $K_s^{(k-1)} < K_s^{(1)}$, i.e., at least one oscillation had occurred during the optimization so far, $K_s^{(k)}$ is increased as follows:

$$K_s^{(k)} = \begin{cases} K_s^{(1)}, & \text{if } \delta_s^{(k)} \geq \delta^{(\max)} \\ a \cdot \delta_s^{(k)} + b, & \text{if } \delta^{(\min)} \leq \delta_s^{(k)} < \delta^{(\max)} \\ K_s^{(k-1)}, & \text{if } \delta_s^{(k)} < \delta^{(\min)} \end{cases} \quad (19)$$

where

$$a = \frac{K_s^{(1)} - K_s^{(k-1)}}{\delta^{(\max)} - \delta^{(\min)}} \quad b = K_s^{(1)} - a \cdot \delta^{(\max)} \quad (20)$$

and $\delta^{(\min)}$ and $\delta^{(\max)}$ are predefined thresholds for the minimum and maximum changes in $S_k^{(+)}$, respectively. The larger $\delta_s^{(k)}$ is, the higher the increase in $K_s^{(k)}$ is. If $\delta_s^{(k)}$ is significantly large, e.g., $\delta_s^{(k)} \geq \delta^{(\max)}$, the value of $K_s^{(k)}$ is restored to its

maximum value $K_s^{(1)}$. Once the value of $K_s^{(k)}$ is changed, the value of $u_{s, dB}^{(k, \max)}$ is updated according to (16). The same procedure can be applied to $S_k^{(-)}$, $T_k^{(+)}$, and $T_k^{(-)}$.

VI. SIMULATION SCENARIO AND PARAMETERS

Here, the simulation scenario is presented along with the parameters of the LTE and 3G networks, and the inter-RAT MRO algorithm.

A. Simulation Scenario

An inter-RAT handover of a UE is necessary when the radio coverage of the connected RAT becomes weak and strong coverage from a different RAT exists. There are two cases where the radio coverage of a RAT is not sufficient: 1) one RAT is deployed only for a limited geographical area, whereas the other RAT is covering the full serving area; and 2) the different frequency bands of LTE and 3G might result in some spots where there is no coverage in one RAT, i.e., a coverage hole mainly caused by physical obstructions (such as buildings, tunnels, and hills) and, at the same time, good coverage from the other one.

To cover the two aforementioned cases, a typical irregular network layout for partly overlaying inter-RAT deployment is used, and coverage holes are placed in both RATs [see Fig. 8(a)]. The complete $9 \times 9 \text{ km}^2$ area (urban and suburban areas) is served by a 3G network, shown in red, whereas LTE covers only the urban area, shown in blue. For clarity, the borders of the sectorized cells are shown without taking the impact of shadowing into account. The total number of sectorized cells is 72, among which 27 are LTE cells and 45 are 3G cells. The identification (ID) number of each cell is shown in Fig. 8(b). ID numbers 1–27 are used for LTE cells (blue) and ID numbers 28 to 72 for 3G cells (red).

Some of the UEs randomly moves in the network, whereas others move at specific trajectories defined by streets. In the scenario, seven street loops are placed in the network, among

TABLE I
NETWORK SIMULATION PARAMETERS

Parameter	Assumptions
Number of cells	LTE: 27 and 3G: 45 cells
Carrier frequency	LTE: 2.6 GHz and 3G: 2.1 GHz
System bandwidth	LTE: 10 MHz and 3G: 5 MHz
Total transmit power	LTE: 40 W and 3G: 20 W (2 W on CPICH)
Shadowing	Standard deviation = 8 dB Decorrelation distance = 50 m Correlation between BSs = 0.5 Correlation between sectors = 1
Fast fading	2-tap Rayleigh fading channel
Noise power	$-174 \text{ dB/Hz} + 10 \cdot \log_{10}(B \text{ [Hz]}) + 7$
Measurement bandwidth	RSRP: 1.25 MHz and RSCP: 5 MHz
L3 measurement filtering	Filter coefficient = 4
Number of UEs	Background : 6 per cell Small street loop : 60 Large street loop : 200
Speed of UEs	Background : 3 km/h Street : 70 km/h
Traffic model	CBR traffic [35] User data rate = 64 kbps
T_T	480 ms

which three are larger than the others [see Fig. 8(a)]. On each of the three large street loops, four alternating LTE and 3G coverage holes are intentionally placed into the simulation landscape, i.e., LTE coverage holes are followed by 3G coverage holes. A coverage hole is created by adding an offset to the shadowing map value at its corresponding location. In particular, the offset is determined, such that the received signal strength, e.g., RSRP or RSCP, falls below -130 and -115 dBm in an LTE and 3G coverage hole, respectively. A ballpark figure for the area of a coverage hole is $60 \times 60 \text{ m}^2$. That is, a UE moving with a speed of 70 km/h would need roughly 4 s to cross diagonally the coverage hole. The cells, which are serving the UEs on these three large street loops, are expected to have a significant number of mobility failure events. The other four small street loops do not have any 3G or LTE coverage holes.

B. Simulation Parameters

In real networks, the collection period T_{KPI} of the values of the KPIs can be on the order of hours, days, and even weeks, depending on the user traffic in the cells. However, in our simulative investigation, T_{KPI} is much smaller and is on the order of 100 s due to limitations in computational complexity. To collect enough mobility failure events from the network during a short period of duration T_{KPI} , a high number of UEs [7], [10] are placed on each street loop. The total number of UEs in the network is set to 1272 and is distributed as follows. Six background UEs are initially placed in each cell, 200 UEs on each of the three large street loops, and 60s UEs on each of the four small street loops. Moreover, to steer the UE from 3G to LTE, the UE performs cell reselection after each RLF and reselects an LTE cell if its corresponding RSRQ is high enough; otherwise, it connects to the 3G network [34].

The rest of the simulation parameters are shown in Table I. The background UEs are randomly moving using a speed of 3 km/h, whereas those moving on the street loops have a speed of 70 km/h. Each UE has a required constant bit rate that is

TABLE II
PARAMETERS USED BY THE INTER-RAT MRO ALGORITHM

Root Cause Analysis		Grouping KPI Counters	
T_{KPI}	100 s	w_s	0.2
$T_{\text{RP}}, T_{\text{QRSQ}}$	3 s	w_t	0.2
T_{HP}	0.25 s		
T_{Qout}	0.5 s		
$Q_{\text{out}}, Q_{\text{fail}}$	-8 dB		
Q_{RSRQ}	-17.7 dB		
Proportional Control Block		Gain Scheduler	
$S^{(\min)}, T^{(\min)}$	20	ρ_s, ρ_t	0.5
$u_{s,\text{dB}}^{(1,\max)}, u_{t,\text{dB}}^{(1,\max)}$	1.5	n_s	3 samples
$e_s^{(\max)}, e_t^{(\max)}$	1.5	$\delta^{(\min)}$	20
$\lambda_{s,\text{dB}}, \lambda_{t,\text{dB}}$	0.5	$\delta^{(\max)}$	40

equal to 64 kbps, according to the model described in [35]. The shadowing is lognormally distributed with a mean of 0 dB and a standard deviation of 8 dB. The fast fading is generated offline according to Jakes' model [36], assuming a two-tap Rayleigh fading channel, i.e., second-order frequency diversity is assumed. Layer 1 (L1) averaging is applied to the physical-layer measurements and is performed differently for the serving and target frequency layers, as described in [37]. Moreover, an independent lognormally distributed measurement error is added to each L1 measurement [38]. The output values of L1 are then filtered using a layer 3 (L3) recursive averaging method applying a filter coefficient equal to 4 [26]. The values of L3, i.e., filtered values of RSRP and RSCP, are used to evaluate the measurement event condition in (2). Note that the RSCP is measured on the full 5-MHz 3G bandwidth with a total transmit power of 2 W on CPICH, i.e., 10% of the total transmit power, whereas the power contribution of each resource element carrying cell-specific reference signal, which is used for RSRP calculation, is measured per 15-kHz chunk.

The parameters that are used by the inter-RAT MRO algorithm are summarized in Table II. In this paper, the default values of $S^{(\min)}$ and $T^{(\min)}$ are set to 20 unless stated otherwise, i.e., the performance of the inter-RAT MRO algorithm is also compared for $S^{(\min)}$ and $T^{(\min)}$ equal to 10. The maximum magnitude of a change $u_{s,\text{dB}}^{(1,\max)}$ or $u_{t,\text{dB}}^{(1,\max)}$ that can be applied to a handover threshold is set to a relatively small value equal to 1.5 dB. The reason for that is to avoid any significant oscillations in the group values and to allow incremental improvements in each KPI period. Moreover, $u_{s,\text{dB}}^{(k)}$ and $u_{t,\text{dB}}^{(k)}$ are further quantized with step sizes $\lambda_{s,\text{dB}} = 0.5$ dB and $\lambda_{t,\text{dB}} = 0.5$, respectively. Weights w_s and w_t used for PPs are both set to 0.2 in this paper, giving more priority for RLFs. As for the gain scheduler, controller gains $K_s^{(k)}$ and $K_t^{(k)}$ are reduced by factors $\rho_s = 0.5$ and $\rho_t = 0.5$, respectively, each time an oscillation in the group values is detected.

VII. SIMULATION RESULTS

Here, the performance of the inter-RAT MRO algorithm is compared with respect to three distinct default network-wide settings of handover thresholds. Moreover, the performance of the inter-RAT MRO algorithm is compared with those obtained by Taguchi's method and simulated annealing.

TABLE III
THREE DISTINCT NETWORK-WIDE SETTINGS OF HANDOVER
THRESHOLDS USED FOR COMPARISON WITH THE OPTIMIZED
SETTINGS OF THE INTER-RAT MRO ALGORITHM

Setting Name	Event B2		Event 3A	
	S_{thr}	T_{thr}	S_{thr}	T_{thr}
A	-129 dBm	-111 dBm	-114 dBm	-126 dBm
B	-125 dBm	-107 dBm	-110 dBm	-122 dBm
C	-118 dBm	-100 dBm	-103 dBm	-115 dBm

A. Evaluation Methodology

The performance of the inter-RAT MRO algorithm is evaluated with respect to the numbers of mobility failure events in each cell and in the whole network. In addition to $N_{\text{PP}}^{(k)}$ and $N_{\text{UH}}^{(k)}$, the total number of RLFs in a cell is denoted by $N_{\text{RLF}}^{(k)}$ in KPI period k . $N_{\text{RLF}}^{(k)}$ is calculated by summing the values of RLF-related KPIs as follows:

$$N_{\text{RLF}}^{(k)} = N_{\text{TLH-S}}^{(k)} + N_{\text{TLH-T}}^{(k)} + N_{\text{TEH}}^{(k)} + N_{\text{HWC}}^{(k)}. \quad (21)$$

Similarly, we denote the total number of RLFs, PPs, and UHs in a network by $T_{\text{RLF}}^{(k)}$, $T_{\text{PP}}^{(k)}$, and $T_{\text{UH}}^{(k)}$ in KPI period k , respectively, i.e., $T_{\text{UH}}^{(k)}$ is exclusive for LTE. $T_{\text{RLF}}^{(k)}$, $T_{\text{PP}}^{(k)}$, and $T_{\text{UH}}^{(k)}$ are calculated by summing $N_{\text{RLF}}^{(k)}$, $N_{\text{PP}}^{(k)}$, and $N_{\text{UH}}^{(k)}$ of all cells belonging to the same RAT, respectively.

The performance of the inter-RAT MRO algorithm is compared with respect to three distinct network-wide settings of handover thresholds, which are shown in Table III. Among the three settings, setting A applies the lowest value of S_{thr} and therefore yields to the largest LTE coverage at the expense of an increase in the probability that a UE experiences an RLF before handing over. On the other hand, the UEs served by cells applying a high value of S_{thr} such as that used in setting C are less vulnerable to TLHs at the expense of a reduction in the LTE coverage and an increase in the number of UHs. Setting B applies a value of S_{thr} , which lies between that of setting A and C, and as result, provides a tradeoff between the LTE coverage and the number of TLHs.

To run the inter-RAT MRO algorithm, the handover thresholds should be initialized. In principle, the convergence of the inter-RAT MRO algorithm should not highly depend on the choice of the initial setting. To investigate the sensitivity of the algorithm with respect to the initial setting, the optimization of the handover thresholds is repeated three times, and in each time, one of the three network-wide settings shown in Table III is used as an initial setting for the handover thresholds. The performance of the inter-RAT MRO algorithm is shown with respect to each cell for only the two initial settings A and C as the results obtained using initial setting B do not provide additional insights. However, the total number of mobility failure events in LTE and 3G networks are shown for all the three network-wide settings and their optimized counterparts.

B. Cell-Specific Performance of the Inter-RAT MRO Algorithm With Respect to Initial Setting A

The numbers of mobility failure events $N_{\text{RLF}}^{(k)}$, $N_{\text{PP}}^{(k)}$, and $N_{\text{UH}}^{(k)}$ are plotted in Fig. 9 as a function of the KPI period k

for all cells having initially or during the optimization mobility problems, i.e., $N_{\text{RLF}}^{(k)}$, $N_{\text{PP}}^{(k)}$, or $N_{\text{UH}}^{(k)}$ exceeds 20 in any KPI period. According to the figure, $6/27 \approx 22\%$ and $4/45 \approx 9\%$ of the LTE and 3G cells, respectively, experience mobility problems. For the mobile operators, it is extremely important to solve the mobility failure events in those limited numbers of cells because the same UEs are constantly experiencing the mobility network errors. Resolving the mobility problems in those cells results in a full gain in terms of user-perceived quality.

In Fig. 9(a), it can be shown that $N_{\text{RLF}}^{(k)}$ of LTE cells 14 and 25 have been completely resolved, whereas those of cells 10 and 19 are reduced approximately by 50% and 70%, respectively, i.e., comparing the values in the first and last KPI periods. The performance of the latter two cells could not be further improved because their corresponding group values $T_k^{(+)}$ and $T_k^{(-)}$ require conflicting actions to be performed on the same handover threshold $T_{\text{thr}}^{(k)}$, e.g., group values of cell 10 are shown in Fig. 10(a). $N_{\text{RLF}}^{(k)}$ of cell 11 did not change during the optimization because its corresponding group value $T_k^{(+)}$ is below the limit $T^{(\min)}$, and in turn, the algorithm did not react on. In Fig. 9(b), it is shown that only LTE cell 14 has experienced an increase in PPs. Similar to the case of cell 11, the algorithm did not react on those PPs because the group values $S_k^{(-)}$ and $T_k^{(+)}$ of cell 14 are below their corresponding limits $S^{(\min)}$ and $T^{(\min)}$, respectively, and they are considered statistically insignificant. As for the UHs, it is shown in Fig. 9(c) that only three LTE cells have small $N_{\text{UH}}^{(k)}$. The reason is that the coverage of the LTE network is well exploited as the cells apply initially a low $S_{\text{thr}}^{(k)} = -129$ dBm at the expense of an increase in $N_{\text{RLF}}^{(k)}$.

As for the 3G network, it is shown in Fig. 9(d) that $N_{\text{RLF}}^{(k)}$ of all the 3G cells have been completely resolved. In addition, only cell 60 has experienced an increase in $N_{\text{PP}}^{(k)}$, as shown in Fig. 9(e). This increase is relatively small, and the algorithm does not react to resolve it. The values of $S_{\text{thr}}^{(k)}$ are shown in Fig. 9(f) as a function of the KPI period k for all the LTE cells of interest. According to the figure, the values of $S_{\text{thr}}^{(k)}$ are increased for all LTE cells 10, 14, 19, and 25, which have initially experienced a high number of RLFs. Moreover, the values of $S_{\text{thr}}^{(k)}$ are cell-specific. The same has been observed for $T_{\text{thr}}^{(k)}$ and for the handover thresholds of 3G cells.

To visualize the importance of the gain scheduler in reducing the oscillations in the group values, an example is depicted in Fig. 10, which shows the behavior of the gain scheduler for LTE cell 10. In the first KPI period, $S_k^{(+)}$ is large, and in turn, threshold $S_{\text{thr}}^{(k)}$ is increased by large $u_{s,\text{dB}} = 1.5$ dB. $S_k^{(+)}$ is completely resolved in KPI period 8, and the algorithm no longer modifies $S_{\text{thr}}^{(k)}$. During the optimization, $T_k^{(+)}$ becomes higher than $T^{(\min)} = 20$ in KPI period 6, and accordingly, $T_{\text{thr}}^{(k)}$ is increased by $u_{t,\text{dB}} = 1.5$ dB until KPI period 16. In KPI period 17, $T_k^{(+)}$ is decreased below $T^{(\min)}$, although at the expense of a significant increase in $T_k^{(-)}$. Apparently, $T_k^{(+)}$ and $T_k^{(-)}$ cannot be both resolved in cell 10 as they both

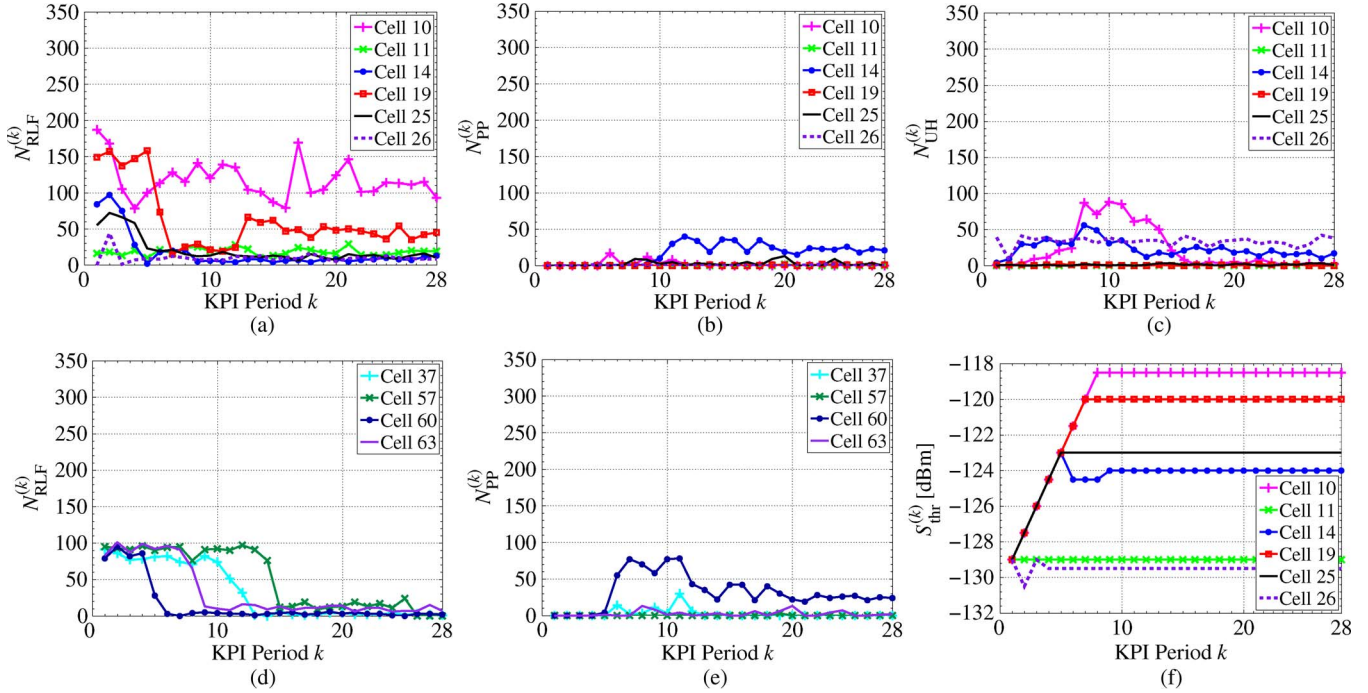


Fig. 9. Performance of the inter-RAT MRO algorithm with respect to initial setting A. (a) Number of RLFs in LTE cells. (b) Number of PPs in LTE cells. (c) Number of UHs in LTE cells. (d) Number of RLFs in 3G cells. (e) Number of PPs in 3G cells. (f) $S_{\text{thr}}^{(k)}$ of LTE cells as a function of k .

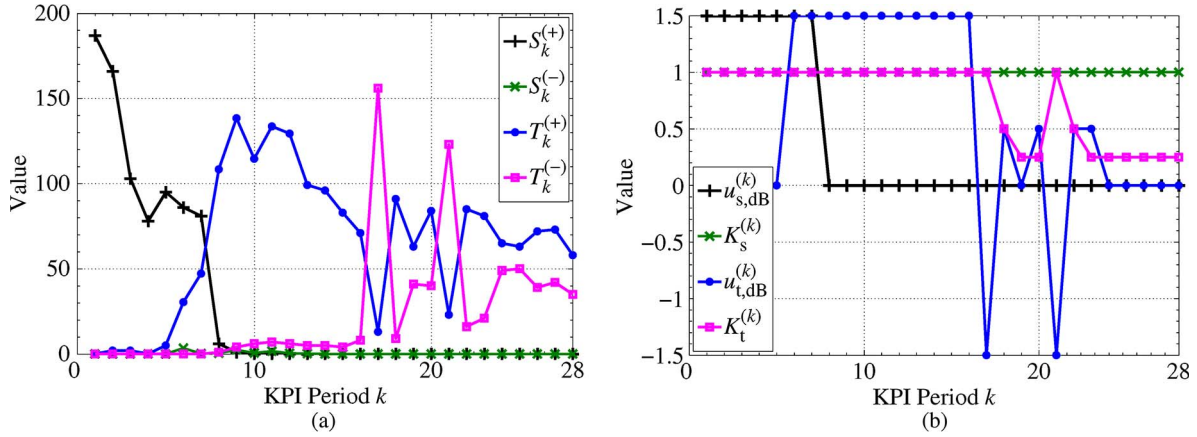


Fig. 10. Example showing the role of the gain scheduler in reducing the oscillations in the group values of cell 10. (a) Group values of cell 10 as a function of the KPI period k . (b) Values of $u_{s,\text{dB}}^{(k)}$ and $u_{t,\text{dB}}^{(k)}$ applied by cell 10 to $S_{\text{thr}}^{(k)}$ and $T_{\text{thr}}^{(k)}$, respectively, and their corresponding controller gains $K_s^{(k)}$ and $K_t^{(k)}$ as a function of the KPI period k .

require conflicting actions to be performed on $T_{\text{thr}}^{(k)}$. In KPI period 18, the gain scheduler detects an oscillation in $T_k^{(+)}$ and $T_k^{(-)}$ and in turn reduces the controller gain $K_t^{(k)}$ by half. The gain scheduler detects a new oscillation in KPI period 19 and reduces furthermore $K_t^{(k)}$. As a result, the magnitude of $u_{t,\text{dB}}^{(k)}$ is reduced from 1.5 dB in KPI period 16 to 0.5 dB in KPI period 18, and to 0 dB in KPI period 19. Therefore, the gain scheduler has gradually learned via detecting the oscillations that a small or no change should be applied to $T_{\text{thr}}^{(k)}$. In KPI period 21, the small change in $T_{\text{thr}}^{(k)}$ yielded again a significant increase in $T_k^{(-)}$, i.e., $\delta^{(21)} > \delta^{(\text{max})}$, and the gain scheduler restores $K_t^{(k)}$ to its maximum value to react on the new mobility failure events. Shortly after, the gain scheduler detects two

oscillations in KPI periods 22 and 23, and reduces again $K_t^{(k)}$ to 0.25. The handover thresholds are not changed in the last five KPI periods, and in turn, stability is achieved in the group values. Without the gain scheduler, $T_k^{(+)}$ and $T_k^{(-)}$ would infinitely oscillate, and stability would not be reached.

C. Cell-Specific Performance of the Inter-RAT MRO Algorithm With Respect to Initial Setting C

The number of mobility failure events $N_{\text{RLF}}^{(k)}$, $N_{\text{PP}}^{(k)}$, and $N_{\text{UH}}^{(k)}$ are plotted in Fig. 11 as a function of the KPI period k for all cells having initially or during the optimization mobility problems. In contrast to initial setting A, the number of LTE cells having significant $N_{\text{RLF}}^{(k)}$ in the first KPI period is smaller

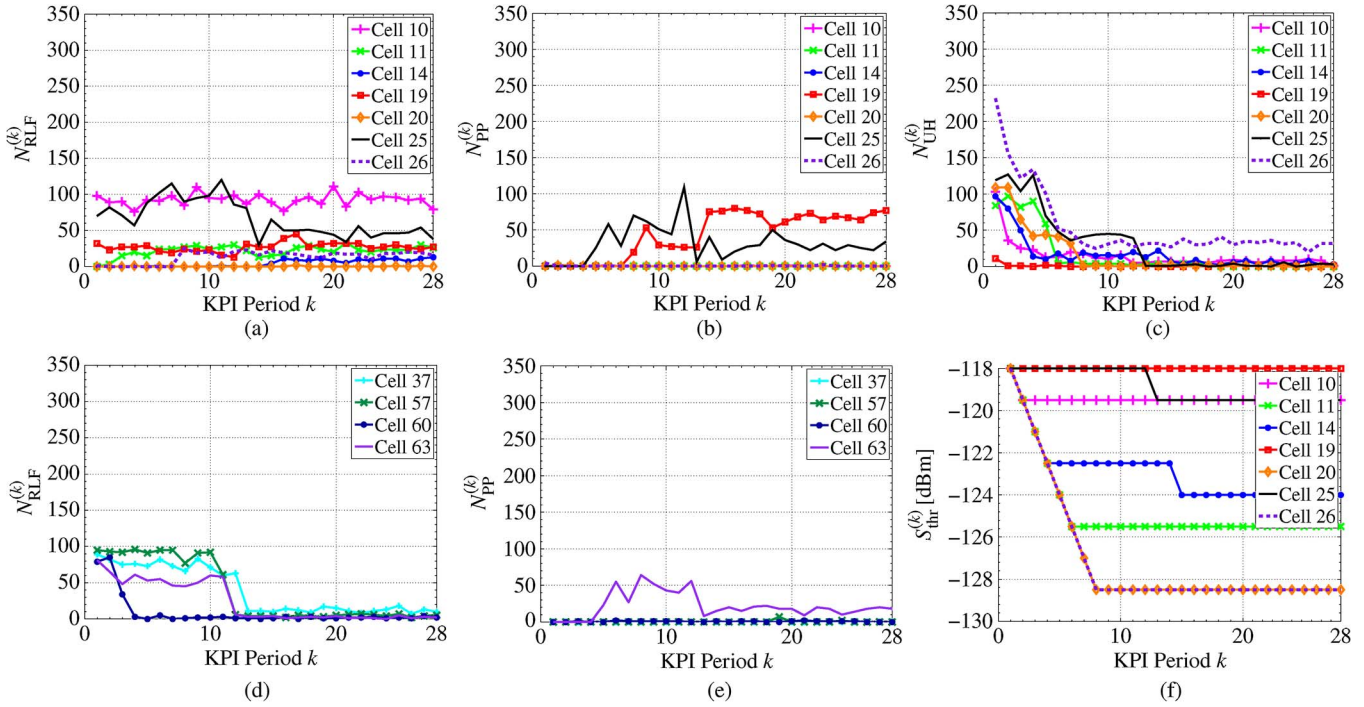


Fig. 11. Performance of the inter-RAT MRO algorithm with respect to initial setting C. (a) Number of RLFs in LTE cells. (b) Number of PPs in LTE cells. (c) Number of UHs in LTE cells. (d) Number of RLFs in 3G cells. (e) Number of PPs in 3G cells. (f) $S_{thr}^{(k)}$ of LTE cells as a function of k .

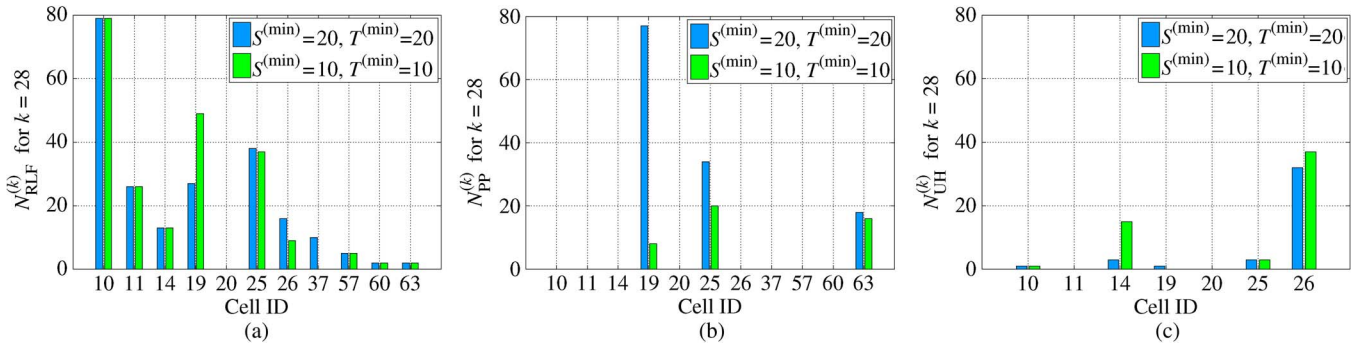


Fig. 12. Performance of the inter-RAT MRO algorithm applying initial setting C for two different values of $S^{(min)}$ and $T^{(min)}$. (a) Number of RLFs. (b) Number of PPs. (c) Number of UHs.

at the expense of an increase in the number of cells having high $N_{UH}^{(k)}$. The reason is that LTE cells initially apply high $S_{thr}^{(k)} = -118$ dBm and in turn are less affected by RLFs at the expense of a reduction in LTE coverage and an increase in $N_{UH}^{(k)}$.

In Fig. 11(a), it is shown that $N_{RLF}^{(k)}$ is reduced for LTE cell 25, whereas the performance of cells 10 and 19 could not be improved as their corresponding group values $T_k^{(+)}$ and $T_k^{(-)}$ require contradicting actions to be performed on $T_{thr}^{(k)}$. The rest of the LTE cells have small $N_{RLF}^{(k)}$ values, which are not large enough for the algorithm to react on. $N_{PP}^{(k)}$ of LTE cells 19 and 25 have increased, as shown in Fig. 11(b); however, the algorithm did not react on them because their corresponding group values did not exceed the minimum limits $S^{(min)}$ and $T^{(min)}$. The inter-RAT MRO algorithm completely resolves the UHs of six LTE cells, as shown in Fig. 11(c). To this end, $S_{thr}^{(k)}$ of the latter LTE cells were decreased cell-specifically, as shown in Fig. 11(f), and consequently, the LTE coverage is expanded. As for the 3G network, $N_{RLF}^{(k)}$ of the 3G cells shown in Fig. 11(d)

have been completely resolved without any significant increase in the number of PPs, as shown in Fig. 11(e).

To investigate the impact of thresholds $S^{(min)}$ and $T^{(min)}$ on the performance of the inter-RAT MRO algorithm, we compare in Fig. 12 the numbers of RLFs, PPs, and UHs of all cells in the last KPI period 28 for two threshold values: $S^{(min)}$ and $T^{(min)}$ are both set either to 10 or 20. According to the figure, it is shown that the latter two threshold values do not have an impact on cells 10, 11, 20, 57, 60, and 63, where similar numbers of mobility failures are achieved. Cells 26 and 37 have less RLFs for $S^{(min)}$ and $T^{(min)}$ equal to 10 at the expense of a slight loss in UHs for cell 26. Moreover, the number of PPs has decreased in cell 25, whereas the number of UHs has increased in cell 14. As for cell 19, the number of PPs has decreased from 77 to 8, i.e., a gain of $(77 - 8) \cdot (w_s + w_t) = 27.6$ in PPs, at the expense of an increase in RLFs from 27 to 49, i.e., a loss of 22 in RLFs. Therefore, the impact of the values of $S^{(min)}$ and $T^{(min)}$ on the overall performance of the inter-RAT MRO algorithm is more or less minimal as long as they are reasonably configured.

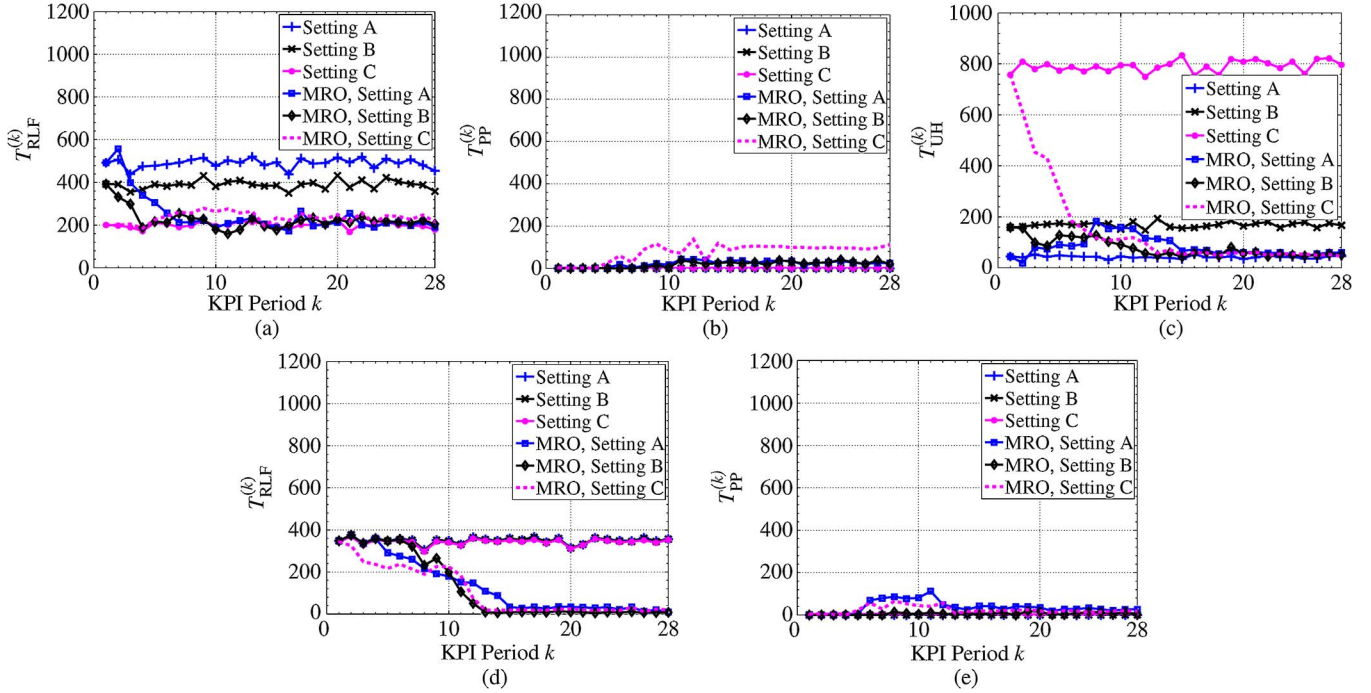


Fig. 13. Comparison between the overall performance of the network-wide settings and their optimized counterparts. (a) Total number of RLFs in the LTE network. (b) Total number of PPs in the LTE network. (c) Total number of UHs in the LTE network. (d) Total number of RLFs in the 3G network. (e) Total number of PPs in the 3G network.

D. Overall Performance of Inter-RAT MRO Algorithm

The performance of the inter-RAT MRO algorithm is compared with respect to the three initial handover settings using the total values of KPIs in each LTE and 3G network.

The inter-RAT MRO algorithm applying initially settings A, B, and C is denoted by MRO settings A, B, and C, respectively. The total number of mobility failure events in LTE and 3G networks is plotted in Fig. 13 for the three network-wide settings A, B, and C and their optimized counterparts. The fluctuations of the network-wide setting curves are statistical fluctuations. According to the figure, it can be observed that the inter-RAT MRO algorithm converges to similar $T_{RLF}^{(k)}$ in LTE and 3G networks, and $T_{UH}^{(k)}$, irrespective of the choice of the initial setting. In Fig. 13(b) and (e), the inter-RAT MRO converges to different $T_{PP}^{(k)}$ depending on the initial setting. However, as discussed in Sections VII-B and VII-C, the inter-RAT MRO does not react on those PPs because their corresponding group values do not exceed the minimum limits $S^{(\min)}$ or $T^{(\min)}$. In other words, any group value that is below the minimum limits is allowed by the inter-RAT MRO algorithm. Hence, the performance of the inter-RAT MRO algorithm is to some extent insensitive to the choice of the initial setting.

For the LTE network, setting A yields the lowest value of $T_{UH}^{(k)}$ but has the largest $T_{RLF}^{(k)}$. In contrast, setting C yields the lowest value of $T_{RLF}^{(k)}$ in LTE but has the largest $T_{UH}^{(k)}$. If compared with the three network-wide settings, the inter-RAT MRO algorithm achieves the lowest $T_{RLF}^{(k)}$ of setting C and the lowest $T_{UH}^{(k)}$ of setting A. The inter-RAT MRO algorithm approximately achieves 50% gains in $T_{RLF}^{(k)}$ in LTE and $T_{UH}^{(k)}$ compared with setting B, which can be considered a tradeoff between settings A and C. As for the 3G network, the network-

wide settings yield a large number of $T_{RLF}^{(k)}$ [see Fig. 13(d)], as opposed to the settings obtained by the inter-RAT MRO algorithm, which resolve completely all the RLF problems in 3G.

The optimized threshold values obtained by the inter-RAT MRO algorithm are shown in Fig. 14 for the three different initial settings. According to the figure, the optimized values of $S_{thr}^{(k)}$ are more or less similar for the different initial settings, whereas the values of $T_{thr}^{(k)}$ are quite different. Therefore, different optimized handover threshold settings can yield the same overall performance, which is shown in Fig. 13. The reason for the difference in the optimized values of the thresholds for some cells is that the inter-RAT MRO algorithm reacts based on the values of collected KPIs, which might differ depending on the applied initial setting. For instance, the RLFs of cell 60 have been all classified as $TLH(T_{thr})$ for initial setting C, and in turn, only $T_{thr}^{(k)}$ is decreased, i.e., $S_{thr}^{(k)}$ is kept fixed. In contrast, portions of RLFs of cell 60 have been classified as $TLH(S_{thr})$ and $TLH(T_{thr})$ for initial settings A and B, and consequently, the serving and target thresholds are modified. We note that all three optimized handover settings of cell 60 have completely resolved the number of RLFs [see Figs. 9(d) and 11(d)].

E. Performance Comparison of the Inter-RAT MRO Algorithm, Taguchi's Method, and Simulated Annealing

The inter-RAT MRO algorithm updates the handover thresholds using logical rules, which are derived from the root-cause analysis of the KPIs. To check the efficiency of the proposed inter-RAT MRO algorithm, its performance is compared with those obtained by two well-known optimization methods: Taguchi's method and simulated annealing, which

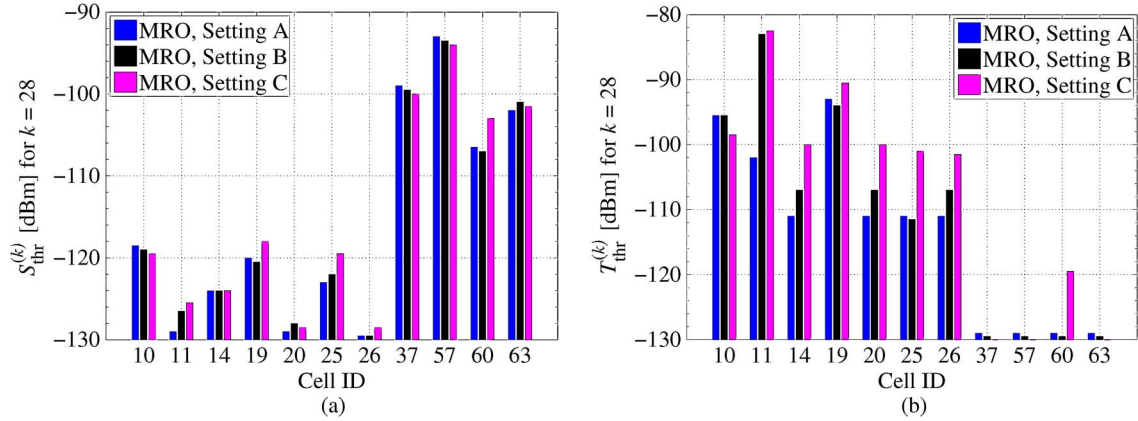


Fig. 14. Optimized threshold values obtained by the inter-RAT MRO algorithm for the three different initial settings. (a) Optimized values of $S_{\text{thr}}^{(k)}$ thresholds. (b) Optimized values of $T_{\text{thr}}^{(k)}$ thresholds.

minimize a predefined cost function. These two methods are not applicable as self-optimizing algorithms in real operating networks because they are based on arbitrary network trials, which may significantly harm the performance of the UE. However, these two optimization methods are used for benchmarking to investigate whether they can converge faster or achieve a lower number of mobility failure events than the inter-RAT MRO algorithm. To this end, the total numbers of RLFs and PPs in both LTE and 3G networks are denoted by $Q_{\text{RLF}}^{(k)}$ and $Q_{\text{PP}}^{(k)}$ in KPI period k , respectively. In this paper, the overall cost function y evaluated in KPI period k is defined as follows:

$$y = Q_{\text{RLF}}^{(k)} + (w_s + w_t) \cdot Q_{\text{PP}}^{(k)} + w_h \cdot T_{\text{UH}}^{(k)} \quad (22)$$

where $w_s = 0.2$, $w_t = 0.2$, and $w_h < 1$ is a weight used for the total number $T_{\text{UH}}^{(k)}$ of UHs in LTE. In this paper, the UHs have lower priority than RLFs, and the inter-RAT MRO algorithm reacts on UHs only if no TLHs occur in the cell. Such an explicit rule for reacting on UHs is not possible for Taguchi's method and simulated annealing, which update the handover thresholds based on the values of a predefined cost function. For this reason, we set $w_h = 0$ and compare the performance of the inter-RAT MRO algorithm with the other two optimization methods, assuming no impact for UHs on the value of the cost function. We denote the vector containing the handover thresholds of all LTE and 3G cells by \mathbf{x} and the value of the cost function y evaluated for \mathbf{x} by $f(\mathbf{x})$.

1) *Taguchi's Method*: Based on the so-called orthogonal array (OA) [22], Taguchi's method selects a reduced set of parameter combinations to be tested from the full search space. The number of selected combinations determines the number of experiments being carried out and evaluated against cost function y . Using all the experimental results, a candidate solution is found, and the process is repeated until a desired criterion is fulfilled. Herein, we use Taguchi's method applying a nearly OA (NOA) rather than an OA since an NOA can be constructed for any number of experiments, and in turn, the complexity of the algorithm can be reduced. NOAs were used in [23] to optimize antenna parameters in eNode B-only deployment within the LTE Rel. 8 framework. In this paper, the NOA used by Taguchi's method consists of 20 experiments;

TABLE IV
OPTIMIZATION RANGE OF EACH HANDOVER THRESHOLD USED BY TAGUCHI'S METHOD AND SIMULATED ANNEALING

	Event B2		Event 3A	
	S_{thr}	T_{thr}	S_{thr}	T_{thr}
Minimum	-129 dBm	-114 dBm	-114 dBm	-129 dBm
Maximum	-97 dBm	-82 dBm	-82 dBm	-97 dBm

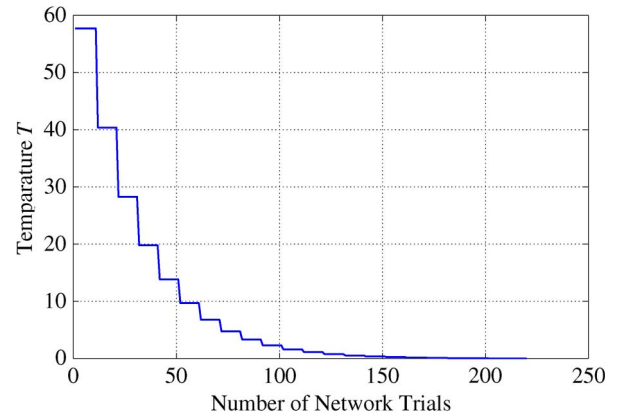


Fig. 15. Value of the temperature T as a function of the number of network trials.

$72 \cdot 2 = 144$ configuration parameters, i.e., each of the 72 cells has two handover thresholds; and five levels [23].

2) *Simulated Annealing*: Simulated annealing is another well-elaborated optimization method that allows nonimproving moves to escape from the local minimum [39]. The method starts by selecting an initial candidate solution $\mathbf{x} = \mathbf{x}_0 \in \Omega$, where Ω is the solution space defined as the set of all feasible candidate solutions. The initial candidate solution \mathbf{x}_0 used by simulated annealing is equal to setting B shown in Table III. In each step or network trial, a new candidate \mathbf{x}' is generated from the neighborhood $\mathcal{N}(\mathbf{x})$ of the current solution: \mathbf{x}' is obtained from \mathbf{x} by adding a random displacement value in the range of ± 3 dB to each element in \mathbf{x} . If $f(\mathbf{x}') \leq f(\mathbf{x})$, \mathbf{x}' is accepted as a current solution in the succeeding step; otherwise, it is accepted with some probability depending on the so-called temperature parameter T and the magnitude of function increase $\delta = f(\mathbf{x}') - f(\mathbf{x})$. This process is repeated until the algorithm converges into a steady state. During the

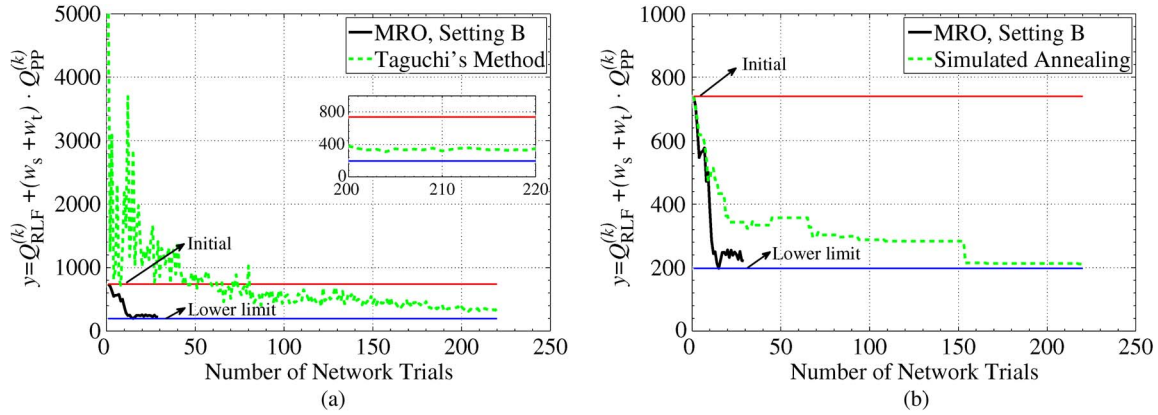


Fig. 16. Comparison between the cost functions achieved by the inter-RAT MRO algorithm applying initial setting B and those obtained by Taguchi's method and simulated annealing. (a) Cost function y as a function of the number of network trials for the inter-RAT MRO algorithm applying initial setting B and Taguchi's method. (b) Cost function y as a function of the number of network trials for the inter-RAT MRO algorithm applying initial setting B and simulated annealing.

search, temperature T is slowly decreased using a standard geometric temperature reduction function $\rho(T) = \kappa \cdot T$ as in [19], where κ is a reduction ratio that is set to 0.7. The initial value of T , denoted by T_0 , is selected such that an increase of 40 in the cost function is accepted at the beginning with a probability of 0.5, i.e., $T_0 = 40 / \log(0.5)$ [23]. The value of T is shown in Fig. 15 as a function of the number of network trials.

3) *Performance Evaluation*: The optimization range of each handover threshold used by Taguchi's method and simulated annealing is shown in Table IV.

The optimization range is defined such that it includes the optimized values of the handover thresholds obtained by the inter-RAT MRO algorithm applying initial setting B. In the case of Taguchi's method, cost function y is evaluated in each experiment, which is equivalent to one network trial. Therefore, one network trial performed by Taguchi's method is equivalent to one evaluation $f(x)$ of the cost function performed by simulated annealing. For both methods, cost function y is evaluated using the values of the KPIs collected from both LTE and 3G networks during the same T_{KPI} time interval used for the inter-RAT MRO algorithm. As for the inter-RAT MRO algorithm, a new set of handover thresholds is selected in each KPI period. Therefore, each KPI period also corresponds to one network trial.

In Fig. 16, cost function y is plotted as a function of the number of network trials for the inter-RAT MRO algorithm applying initial setting B, Taguchi's method in Fig. 16(a), and simulated annealing in Fig. 16(b). The red line indicates the value of the cost function evaluated in the first KPI period for the network-wide setting B. The blue line determines the minimum value of the cost function that the inter-RAT MRO algorithm applying initial setting B converges to during the optimization. Simulated annealing has the same cost function of the inter-RAT MRO algorithm in the first KPI period since it applies setting B as initial candidate solution x_0 . However, Taguchi's method does not have any initial setting [23], and in turn, the value of its cost function in the first KPI period is different than those of simulated annealing and the inter-RAT MRO algorithm.

According to Fig. 16, it is shown that the inter-RAT MRO algorithm has a much faster convergence than Taguchi's method and simulated annealing. This is because the inter-RAT MRO directly reacts on the handover thresholds of the cells having mobility problems, whereas the two other methods explore first the predefined optimization range of the handover threshold before converging. Moreover, the minimum values of the cost functions achieved by the inter-RAT MRO algorithm, Taguchi's method, and simulated annealing are 73.3%, 52.7%, and 71.49% lower than the cost function of the network-wide setting B shown by the red line, respectively. Therefore, the inter-RAT MRO algorithm outperforms in this scenario Taguchi's method and provides comparable results to simulated annealing. This result, indeed, shows that the logical decisions that are used by the inter-RAT MRO algorithm to adjust the handover thresholds are appropriate and efficient.

VIII. CONCLUSION AND OUTLOOK

In this paper, a SON-based algorithm for optimizing inter-RAT handover thresholds has been presented. The algorithm runs on both LTE and 3G networks. The inter-RAT KPIs are defined and the root cause of each mobility failure event is determined. An inter-RAT handover is triggered by a dual-threshold measurement event where the first threshold corresponds to the serving cell and the second threshold to the neighboring target cell of another RAT. As a result, there are two types of too-late handovers in contrast to the intra-RAT case, where a single type of too-late handover exists. The values of the inter-RAT KPIs are collected from each cell in both RATs and are further mapped into four new other values depending on the action required by each mobility failure event, i.e., increasing or decreasing a handover threshold. Modifying the handover thresholds by a fixed and large step size may lead to fluctuations in the values of the KPIs and, in turn, instability in the network. As a countermeasure, a proportional feedback controller is used to apply the necessary amount of change to each handover threshold. Moreover, a gain scheduler is added to adjust the parameters of the controller according to the mobility conditions of each cell.

Simulation results have shown that the optimized handover thresholds obtained by the inter-RAT MRO algorithm outperform three distinct network-wide settings of handover thresholds. In addition, the results demonstrate the necessity of cell-specific handover thresholds depending on the mobility and traffic conditions in different handover areas. Moreover, it is shown that the performance of the proposed inter-RAT MRO algorithm is, to some extent, independent of the choice of the initial setting of the handover thresholds. The performance of the inter-RAT MRO algorithm is compared with those obtained by two other optimization methods: Taguchi's method and simulated annealing. Results have shown that the inter-RAT MRO algorithm converges much faster than Taguchi's method and simulated annealing. Moreover, the algorithm has achieved a value of the cost function, which is lower than that of Taguchi's method and comparable to that of simulated annealing. This indeed validates the efficiency and the correctness of the logical decisions used by the proposed inter-RAT MRO algorithm to update the handover thresholds.

As a future work, the inter-RAT MRO algorithm will be extended to include additional mobility-related parameters affecting the inter-RAT handovers, such as filter coefficient, TTT, and the cell-pair specific handover offsets. The prospective studies will investigate whether the optimization of these additional parameters will further improve mobility performance.

REFERENCES

- [1] M. Rahnema, *UMTS Network Planning, Optimization and Inter-Operation With GSM*. Hoboken, NJ, USA: Wiley, 2008.
- [2] J. Belschner, P. Arnold, H. Eckhardt, E. Kuhn, E. Patouni, A. Kousaridas, N. Alonistioti, A. Saatsakis, K. Tsagkaris, and P. Demestichas, "Optimization of radio access network operation introducing self-x functions: Use cases, algorithms, expected efficiency gains," in *Proc. IEEE Veh. Technol. Conf.*, Apr. 2009, pp. 1–5.
- [3] I. Forkel, M. Schmocker, L. Lazin, M. Becker, F. Debus, and F. Winnewisser, "Cell-specific optimized parameterization of compressed mode operation and inter-system handovers in UMTS/GSM overlay networks," in *Proc. Eur. Wireless*, Paris, France, Apr. 2007, pp. 1–7.
- [4] C. Brunner, A. Garavaglia, M. Mittal, M. Narang, and J. Bautista, "Inter-system handover parameter optimization," in *Proc. IEEE Veh. Technol. Conf.*, Sep. 2006, pp. 1–6.
- [5] 3rd Generation Partnership Project, Self-Configuring and Self-Optimizing Network use Cases and Solutions, Sophia-Antipolis, France, Tech. Rep. TR 36.902, 2009.
- [6] I. Viering, B. Wegmann, A. Lobinger, A. Awada, and H. Martikainen, "Mobility robustness optimization beyond Doppler effect and WSS assumption," in *Proc. IEEE Int. Symp. Wireless Commun. Syst.*, Aug. 2011, pp. 1–6, Invited Paper.
- [7] Z. Wei, "Mobility robustness optimization based on UE mobility for LTE system," in *Proc. IEEE Int. Conf. Wireless Commun. Signal Process.*, Oct. 2010, pp. 1–5.
- [8] T. Jansen, I. Balan, J. Turk, I. Moerman, and T. Kürner, "Handover parameter optimization in LTE self-organizing networks," in *Proc. IEEE Veh. Technol. Conf. Fall*, Sep. 2010, pp. 1–5.
- [9] T. Jansen, I. Balan, S. Stefanski, I. Moerman, and T. Kürner, "Weighted performance based handover parameter optimization in LTE," in *Proc. IEEE Veh. Technol. Conf.*, May 2011, pp. 1–5.
- [10] I. Balan, T. Jansen, B. Sas, I. Moerman, and T. Kürner, "Enhanced weighted performance based handover optimization in LTE," in *Proc. Future Netw. Mob. Summit*, Jun. 2011, pp. 1–8.
- [11] A. Awada, B. Wegmann, D. Rose, I. Viering, and A. Klein, "Towards self-organizing mobility robustness optimization in inter-RAT scenario," in *Proc. IEEE Int. Workshop Self-Organizing Netw.*, May 2011, pp. 1–5.
- [12] A. Awada, B. Wegmann, I. Viering, and A. Klein, "Self-optimization algorithm for inter-RAT configuration parameters," in *Proc. IEEE Int. Symp. Wireless Commun. Syst.*, Aug. 2011, pp. 311–316.
- [13] U. Bakshi and M. V. Bakshi, *Modern Control Theory*. Pune, India: Technical Publ., 2008.
- [14] R. Palm, D. Driankov, and H. Hellendoorn, *Model Based Fuzzy Control*. Berlin, Germany: Springer-Verlag, 1997.
- [15] P. Loannou and B. Fidan, *Adaptive Control Tutorial*. Philadelphia, PA, USA: SIAM, 2006.
- [16] W.-C. Weng, F. Yang, and A. Elsherbeni, "Linear antenna array synthesis using Taguchi's method: A novel optimization technique in electromagnetics," *IEEE Trans. Antennas Propag.*, vol. 55, no. 3, pp. 723–730, Mar. 2007.
- [17] D. Henderson, S. H. Jacobson, and A. Johnson, *The Theory and Practice of Simulated Annealing*. Norwell, MA, USA: Kluwer, 2003.
- [18] I. Siomina and D. Yuan, "Enhancing HSDPA performance via automated and large-scale optimization of radio base station antenna configuration," in *Proc. IEEE Veh. Technol. Conf.*, May 2008, pp. 2061–2065.
- [19] S. Hurley, "Planning effective cellular mobile radio networks," *IEEE Trans. Veh. Technol.*, vol. 51, no. 2, pp. 243–253, Mar. 2002.
- [20] R. Roy, *Design of Experiments Using the Taguchi Approach: 16 Steps to Product and Process Improvement*. Hoboken, NJ, USA: Wiley, 2001.
- [21] Y. Cai and D. Liu, "Multiuser detection using the Taguchi method for DS-SS-CDMA systems," *IEEE Trans. Wireless Commun.*, vol. 4, no. 4, pp. 1594–1607, Jul. 2005.
- [22] A. Awada, B. Wegmann, I. Viering, and A. Klein, "Optimizing the radio network parameters of the long term evolution system using Taguchi's method," *IEEE Trans. Veh. Technol.*, vol. 60, no. 8, pp. 3825–3839, Oct. 2011.
- [23] A. Awada, B. Wegmann, I. Viering, and A. Klein, "A joint optimization of antenna parameters in a cellular network using Taguchi's method," in *Proc. IEEE Veh. Technol. Conf.*, May 2011, pp. 1–5.
- [24] O. Bulakci, A. Awada, A. Bou Saleh, S. Redana, J. Hamalainen, B. Wegmann, B. Raaf, and I. Viering, "Joint optimization of uplink power control parameters in LTE-advanced relay networks," in *Proc. IEEE Wireless Commun. Mob. Comput. Conf.*, July 2011, pp. 2064–2069.
- [25] O. Bulakci, A. Awada, A. Bou Saleh, S. Redana, and J. Hamalainen, "Automated uplink power control optimization in LTE-advanced relay networks," *EURASIP J. Wireless Commun.*, vol. 2013, no. 1, p. 8, Jan. 2013.
- [26] 3rd Generation Partnership Project, Evolved Universal Terrestrial Radio Access (E-UTRA); Radio Resource Control (RRC); Protocol Specification, Sophia-Antipolis, France, Tech. Rep. TS 36.331, 2009.
- [27] 3rd Generation Partnership Project, Technical Specification Group Radio Access Network; Radio Resource Control (RRC); Protocol Specification, Sophia-Antipolis, France, Tech. Rep. TS 25.331, 2010.
- [28] 3rd Generation Partnership Project, Technical Specification Group Radio Access Network; Physical Layer; Measurements (FDD), Sophia-Antipolis, France, Tech. Rep. TR 25.215, 2011.
- [29] J. Kurjenniemi and T. Henttonen, "Effect of measurement bandwidth to the accuracy of inter-frequency RSRP measurements in LTE," in *Proc. IEEE Symp. Pers., Indoor Mob. Radio Commun.*, Sep. 2008, pp. 1–5.
- [30] 3rd Generation Partnership Project, 3 GPP TSG SA WG5, 32.425 CR0089. [Online]. Available: www.3gpp1.org/ftp/tsg_sa/WG5_TM/TSGS5_79/Docs/S5-113108
- [31] 3rd Generation Partnership Project, Technical Specification Group Services and System Aspects; Telecommunication Management, Performance Management; Performance Measurements (E-UTRA), Sophia-Antipolis, France, Tech. Rep. TS 32.425, V11.3.0, 2012.
- [32] 3rd Generation Partnership Project, Evolved Universal Terrestrial Radio Access (E-UTRA) and Evolved Universal Terrestrial Radio Access Network (E-UTRAN); Overall Description, Sophia-Antipolis, France, Tech. Rep. TS 36.300, V11.3.0, 2012.
- [33] 3rd Generation Partnership Project, 3GPP TSG RAN3, 36.300 R3-103485. [Online]. Available: www.3gpp.org/ftp/tsg_ran/WG3_Iu/TSGR3_70/Docs/R3-103485
- [34] 3rd Generation Partnership Project, Evolved Universal Terrestrial Radio Access (E-UTRA); User Equipment (UE) Procedures in Idle Mode, Sophia-Antipolis, France, Tech. Rep. TS 36.304, 2011.
- [35] I. Viering, M. Döttling, and A. Lobinger, "A mathematical perspective of self-optimizing wireless networks," in *Proc. IEEE Int. Conf. Commun.*, Jun. 2009, pp. 1–6.
- [36] W. C. Jake, *Microwave Mobile Communications*. Hoboken, NJ, USA: Wiley, 1974.
- [37] 3rd Generation Partnership Project, Evolved Universal Terrestrial Radio Access (E-UTRA); Requirements for Support of Radio Resource Management, Sophia-Antipolis, France, Tech. Rep. TS 36.133, 2010.
- [38] M. Anas, F. D. Calabrese, P.-E. Östling, K. I. Pederson, and P. E. Mogensen, "Performance analysis of handover measurements and layer 3 filtering for Utran LTE," in *Proc. IEEE Symp. Pers., Indoor Mob. Radio Commun.*, Sep. 2007, pp. 1–5.
- [39] S. Kirkpatrick, C. D. Gelatt, and M. P. Vecchi, "Optimization by simulated annealing," *Science*, vol. 220, no. 4598, pp. 671–680, May 1983.



Ahmad Awada (M'12) received the B.E. degree in computer and communication engineering from the American University of Beirut, Beirut, Lebanon, in 2007 and the M.S. degree in communication engineering from the Technical University of Munich, Munich, Germany, in 2009. He is currently working toward the Ph.D. degree with the Department of Communication Technology, Darmstadt University of Technology, Darmstadt, Germany.

Since 2009, he has been conducting his research activities with the Department of Radio Systems, Nokia Siemens Networks, Munich, Germany. His research interests include self-organizing networks and network optimization processes.



Ingo Viering (M'09) received the Dipl.-Ing. degree from Darmstadt University of Technology, Darmstadt, Germany, in 1999 and the Dr.-Ing. degree from the University of Ulm, Ulm, Germany, in 2003.

In 2002, he was with the Telecommunications Research Center Vienna, Vienna, Austria, where he conducted early measurements of multiple-input-multiple-output channels. He was a Consultant with Siemens in all air-interface-related research areas. Then, in 2004, he cofounded Nomor Research GmbH, Munich, Germany, where he is currently the acting Chief Executive Officer. Since 2007, he has been a Senior Lecturer with the Technical University of Munich, Munich, Germany. Among other things, he supervised collaborations with universities and backofficing Third Generation Partnership Project standardization, and was involved in the early evaluation of emerging technologies, such as fast low-latency access with seamless handoff-orthogonal frequency-division multiplexing, Worldwide Interoperability for Microwave Access, and Long Term Evolution. He is the author of more than 50 scientific papers and the holder of 60 patents.

Dr. Viering was a recipient of the VDE Award for the achievements of Nomor Research from the Association for Electrical, Electronic and Information Technologies (VDE) in 2009.



Bernhard Wegmann received the Dipl.-Ing. and Dr.-Ing. (Ph.D.) degrees in communication engineering from the Technical University of Munich, Munich, Germany, in 1987 and 1993, respectively.

In 1995, he joined the Communications Group, Siemens AG, where he has worked with different departments, such as in research and development, standardization, strategic product management, and network engineering. After the merger of the Communication Group, Siemens AG and the Network Group, Nokia, in April 2007, he moved to Nokia Siemens Networks, Munich, Germany, where he is currently with the Research Group for Future Mobile Radio Systems, dealing with Long-Term Evolution (LTE) and LTE Advanced standardization research. His research interests include radio transmission techniques, radio resource management, self-organizing networks, and radio network deployment.



Anja Klein (M'95) received the Dipl.-Ing. and Dr.-Ing. (Ph.D.) degrees in electrical engineering from the University of Kaiserslautern, Kaiserslautern, Germany, in 1991 and 1996, respectively.

From 1991 to 1996, she was a member of the staff of the Research Group for Radio-Frequency Communications with the University of Kaiserslautern. In 1996, she joined the Mobile Networks Division, Siemens AG, Munich and Berlin, Germany. There, she was active in the standardization of third-generation mobile radio in the European Telecommunications Standards Institute and in the Third-Generation Partnership Project (3GPP), for instance, leading the Time-Division Duplexing Group in RAN1 of the 3GPP. She was also the Vice President of the Department of Development and the Department of Systems Engineering. Since May 2004, she has been with the Darmstadt University of Technology, Darmstadt, Germany, as a Full Professor, heading the Communications Engineering Laboratory. She is the author of over 200 refereed papers and a Contributor for ten books. She is the inventor or co-inventor of more than 45 patents in the field of mobile radio. Her main research interests include mobile radio, multi-antenna systems, radio resource management, interference management, relaying and multihop, cooperative communication, network planning, and cross-layer design.

Dr. Klein is a member of the Association for Electrical, Electronic, and Information Technologies-Information Technology Society. She received the Inventor of the Year Award from Siemens AG in 1999.